Three Muscle-Specific DAF-16/FOXO Transcriptional Targets Activated by Reduced Insulin/IGF-1 Signaling

Shifei Wu[1,2], Jinghua Gao[1,2], Yan Li[2], Charline Roy[3], Ying Wang[2], Ben Mulcahy[2], William Li[1,2], Sruthy Ravivarma[2,4], John Calarco[4], Wesley Hung[2,5], Mei Zhen[1,2,4,5]

[1]Department of Molecular Genetics, University of Toronto, Toronto, ON M5S 3K3, Canada
[2]Lunenfeld-Tanenbaum Research Institute, Mount Sinai Hospital, Toronto, ON M5G 1X5, Canada
[3]Institut NeuroMyoGène, MeLiS, CNRS UMR 5284, INSERM U1314, Université Claude Bernard Lyon 1, Université de Lyon, Lyon, France
[4]Department of Cell and Systems Biology, University of Toronto, Toronto, ON M5S 3G5, Canada
[5]Correspondence: hung@lunenfeld.ca; meizhen@lunenfeld.ca

Keywords: insulin signaling, DAF-16/FOXO, tissue specificity

Abstract

C. elegans insulin/insulin-like growth factor 1 signaling, IIS, affects diverse physiological processes through the DAF-16/FOXO transcription factor. Despite its ubiquitous presence in somatic cells, DAF-16's effects exhibit prevalent tissue specificity as well as tissue crosstalk. This implies that tissue-specific DAF-16 transcriptional programs contribute to functional diversity of IIS. To further investigate this possibility, we sought muscle-cell-specific DAF-16 transcriptional targets. Using fluorescence-activated cell sorting to enrich for body wall muscle cells from young hermaphroditic adults, we compared the muscle cell mRNA transcriptomes under conditions of high and low IIS activity, with and without DAF-16. We further analyzed DAF-16a's binding sites in muscle and intestine cells by chromatin-immunoprecipitation sequencing. Combined output of these analyses is 12 candidate DAF-16 targets enriched for muscle cells. Transcriptional and translational reporters for three out of the four top candidates - a secreted protein C54F6.5, a calcium-binding protein CEX-1/calexcitin, and a fatty acid metabolic enzyme MLCD-1/MCD - showed DAF-16-dependent activation specifically in body wall muscle cells. Notably, reporters for *C54F6.5* and *cex-1* exhibit DAF-16-independent, constitutive expression in non-muscle cells, explaining their low rank or absence from the DAF-16 target lists generated by whole-animal microarray or mRNA-sequencing analyses. These results highlight the need to examine FOXO targets in a cell-type-specific manner.

Article Summary

This study is relevant to those interested in functional specificity of signaling pathways. It describes a rigorous workflow to identify tissue-specific transcriptional changes activated by DAF-16/FOXO, a key effector of insulin signaling, its tissue-specific chromatin binding sites, and experimental validation of three previously unknown DAF-16 targets in body wall muscle cells. These findings highlight the intricacy of tissue-specific regulation exerted by a signaling pathway that is present and operates across tissues.

58 **Introduction**

59 The insulin/insulin-like growth factor 1 (IGF-1) signaling (IIS) regulates a variety of
60 physiological functions (Rask-Madsen and Kahn 2012), from developmental decision (Gottlieb
61 and Ruvkun 1994; Morris et al. 1996; Kimura et al. 1997; Kaletsky and Murphy 2010), neural
62 development (Man et al. 2000; Mielke et al. 2005; Plum et al. 2006; Chiu and Cline 2010;
63 Klöckener et al. 2011; Nieto-Estévez et al. 2016), learning (Kodama et al. 2006; Tomioka et al.
64 2006; Lin et al. 2010; Oda et al. 2011; Chen et al. 2013; Tomioka et al. 2016), aging (Pan et al.
65 2011; Tank et al. 2011; Toth et al. 2012; Liu et al. 2013; Hahm et al. 2015; Li et al. 2019; Weng
66 et al. 2024), longevity (Kenyon et al. 1993; Kimura et al. 1997; Ogg et al. 1997; Kaletsky and
67 Murphy 2010), to stress response (McColl et al. 2010; Rasulova et al. 2021). Key components of
68 the canonical IIS signaling pathway, consisted of the insulin and insulin-like ligands (INS), their
69 respective transmembrane tyrosine kinase receptors, the cascade of phosphoinositide 3-kinase
70 (PI3K) and serine/threonine kinase transducer of the receptor activity, and the effector of
71 phosphorylation, the FOXO transcription factor, are conserved across animals (Kleemann and
72 Murphy 2009; Piñero González et al. 2009; Kaletsky and Murphy 2010; Kenyon 2010).
73 IIS and its physiological functions have been extensively investigated in *C. elegans*. Compared
74 to other systems, *C. elegans* has significantly expanded genes encoding INS (Pierce et al. 2001:
75 20; Li et al. 2003: 28), while keeping a single, ancestral receptor DAF-2/InR for INS (Kenyon et
76 al. 1993; Kimura et al. 1997). With remarkable complexity in their spatial and temporal
77 expression pattern (Liu et al. 2014), 39 INS homologs (INS 1-37, INS-39 and DAF-28) either
78 positively or negatively regulate the IIS activity (Chen et al. 2013; Hung et al. 2013; Murphy
79 2013; Fernandes de Abreu et al. 2014; Hung et al. 2014; Liu et al. 2014; Zhu and Chin-Sang
80 2024). An activated DAF-2 receptor activates a conserved PI3K (AGE-1) (Morris et al. 1996),
81 PDK (PDK-1), and AKT (AKT-1 and AKT-2) (Paradis and Ruvkun 1998; Paradis et al. 1999)
82 kinase cascade, leading to phosphorylation and cytoplasmic retention of the FOXO (DAF-16)
83 transcription factor, inhibiting its transcriptional activity (Gottlieb and Ruvkun 1994; Ogg et al.
84 1997; Henderson and Johnson 2001; Lee et al. 2001; Libina et al. 2003; Lin et al. 2010) (Figure
85 1a). Consistent with IIS participating in diverse cellular functions, molecular components of the
86 signaling cascade (from DAF-2/InR to DAF-16/FOXO) are expressed across cell-types
87 (Aghayeva et al. 2021). Like the case for other signaling pathways, this raises a challenging
88 mechanistic question: how does a single signaling cascade achieve its functional specificity?

89 Previous studies showed that functional specificity of *C. elegans* IIS results in part from the
90 partial overlap of cells that produce different combination of INS (Murphy 2013). We and others
91 further speculated that DAF-16 may define cell autonomous and non-autonomous functions of
92 IIS by accessing different sets of transcriptional targets in a tissue-specific manner. Indeed,
93 several processes regulated by IIS activity exhibit prominent tissue-specificity. A decreased IIS
94 activity leads to increased adult lifespan (Kenyon et al. 1993; Kimura et al. 1997; Ogg et al.
95 1997; Kaletsky and Murphy 2010), and promotes an alternative 'dauer' developmental state that
96 confers resistance to starvation and dehydration (Gottlieb and Ruvkun 1994; Morris et al. 1996;
97 Kimura et al. 1997; Kaletsky and Murphy 2010). Both processes exhibit a strong requirement for
98 an increased DAF-16 activity in the intestine. DAF-16's presence in interneurons affect salt-
99 associated learning (Kodama et al. 2006; Tomioka et al. 2006; Lin et al. 2010; Oda et al. 2011;
100 Chen et al. 2013; Tomioka et al. 2016). In motor neurons, decreased IIS and subsequent
101 activation of DAF-16 functions cell-autonomously to delay age-related decline in axon
102 regeneration (Byrne et al. 2014). Even more intriguingly, IIS from both neurons and muscles
103 contribute to age-dependent motility decline, but in opposite ways, at different phases of
104 adulthood (Hahm et al. 2015; Roy et al. 2022).
105 DAF-16 regulates many critical processes in muscles, including synapse-targeting process
106 (muscle arm) extension (Dixon et al. 2008), neuromuscular junction maturation (Hung et al.
107 2013), cell death prevention (Oh and Kim 2013), and heat-induced calcium overload resistance
108 (Momma et al. 2017). Consistent with observations in other tissues, DAF-16 plays both
109 autonomous and non-autonomous roles in muscle cells (Zhang et al. 2013). Cell-autonomous
110 functions of DAF-16 might be explained by DAF-16's transcriptional regulation of muscle-
111 specific targets; on the other hand, inter-tissue communication might be mediated through its
112 targets that either are secreted from muscles, or residing at the muscle surface to affect the
113 development of other cells.
114 To date, efforts to identify DAF-16 targets have focused on measuring differential gene
115 expression in the presence or absence of active DAF-16 in whole animals. Using either
116 microarrays or mRNA-sequencing (mRNA-seq), these studies identified transcriptional changes
117 relate to metabolism, oxidative-stress response, lifespan, and development (McElwee et al. 2003;
118 Murphy et al. 2003; Lee et al. 2009; Kaplan et al. 2015; Hibshman et al. 2017). Towards the
119 identification of tissue-specific DAF-16 targets, transcriptome profiling on all neuronal cells

120 identified enriched transcripts; many were shown or speculated to participate in age-related
121 memory decline or axon regeneration and learning (Kaletsky et al. 2016; Weng et al. 2024).
122 However, comprehensive information on DAF-16 targets in a cell-type-specific manner is
123 lacking.
124 Obtaining a list of high-confidence transcriptional targets of DAF-16 in a cell-type specific
125 manner is a prerequisite for the mechanistic dissection on how IIS regulates diverse
126 physiological processes in different cells. We want to contribute towards this goal by identifying
127 DAF-16 targets specific for the body wall muscle cells. Our focus on muscle cells was motivated
128 in part by the abundance and homogeneity of this tissue, and in part by the availability of raw
129 DAF-16::GFP chromatin immunoprecipitation sequencing (ChIP-seq) datasets for the muscle
130 cells (Kudron et al. 2018). We generated multiple FACS-sorted muscle cell bulk mRNA-seq
131 datasets and combined them with available tissue-specific ChIP-seq (one muscle-specific and
132 two intestine-specific) datasets to identify high-confidence muscle-enriched DAF-16
133 transcriptional targets. Reporters for top three candidates confirmed muscle-specific DAF-16-
134 dependent expression. Overall, this study contributes towards understanding of how biology
135 utilizes a limited number of signaling pathways to build richly diverse life forms.
136

137 **Materials and methods**

138 **Strains and transgene generation**

139 *C. elegans* strains were cultured on OP50-seeded NGM media (Brenner 1974) at 22.5°C (unless
140 otherwise stated). *daf-2(e1370)* temperature-sensitive animals were cultured at the permissive
141 temperature 15°C and shifted to the restrictive temperature for experiments (see below for details
142 for each experiment). A list of strains and plasmids used in this study is provided in Table S1.
143 Transgenic animals were generated by microinjection as described previously (Mello and Fire
144 1995). For plasmid-based reporters, stable extrachromosomal arrays of each reporter construct
145 were generated and assessed for consistency of expression patterns. Afterwards, one stable
146 extrachromosomal array of each reporter was crossed into *daf-16(lf)*, *daf-2(lf), daf-16(lf)*; *daf-*
147 *2(lf)* for quantification purposes. Endogenous reporters for *gstk-2(syb5762)* and *cex-1(syb8040)*
148 were generated by CRISPR-Cas9 (SunyBiotech) and outcrossed against N2 for at least four
149 times.
150

151 **Transcriptional and translational reporter plasmid construction**

152 *C54F6.5*: Two transcriptional (pJH4768, pJH5155) and two translational (pJH4815, pJH5133)
153 reporters were examined. For transcriptional reporters, a promoter sequence (1225 bp upstream
154 of its start codon and the first 106 bp of its coding sequence) was generated with PCR from wild-
155 type genomic DNA. It was cloned into the Fire Vector that supplied a generic 3' UTR derived
156 from *unc-54* (a gift from Andrew Fire; Addgene kit # 1000000001) to create pJH4768. A
157 *C54F6.5* 3' UTR fragment (1.6 kb downstream of its stop codon) was generated with PCR from
158 wild-type genomic DNA to replace the generic 3' UTR of pJH4768 to generate pJH5155. For
159 translational reporters, the remainder of C54F6.5 coding sequence was synthesized (IDT) and
160 introduced into pJH4768 by Gibson Assembly to generate pJH4815, and into pJH5155 to
161 generate pJH5133.

162 *cex-1*: *cex-1* 3' UTR (1053 bp downstream of its stop codon) was used to replace the *unc-54* 3'
163 UTR in a previously described P_{cex-1} mCherry reporter that contains 2862 bp upstream of its start
164 codon (Ji et al. 2021) to generate the transcriptional reporter pJH4782. An endogenous
165 translational reporter (*syb8040*) was generated by in-frame insertion of RFP::AID at the start
166 codon.

167 *mlcd-1*: 949 bp upstream of its start codon and 990 bp downstream of its stop codon were
168 included as its promoter and 3' UTR sequence, respectively, to generate a transcriptional GFP
169 reporter, pJH5134.

170 *gstk-2*: An endogenous transcription reporter *syb5762* was generated by inserting a *sl2-gfp*
171 reporter after the C-terminal stop codon of the *gstk-2* genomic locus.

172

173 **FACS isolation of muscle cells and mRNA-seq preparation**

174 Wild-type and *daf-16(lf)* worms with GFP-labeled muscles (Table S1, JAC127 and ZM9156)
175 were synchronized and grown at 22.5°C throughout development until they became young
176 adults. *daf-2(lf)* and *daf-16(lf); daf-2(lf)* animals with GFP-labeled muscles (Table S1, ZM10379
177 and ZM10380) were synchronized, grown at 15°C until L4 to prevent dauer formation during
178 L1-L2 transition and molting arrest in larva stage afterwards exhibited by *daf-2(lf)*, and shifted to
179 22.5°C to activate DAF-16 for 8 hours. From these synchronized young adult worms, cells were
180 extracted with SDS-DTT, dissociated with pronase, and filtered through a 20 μm cell strainer
181 (Spencer et al. 2014). FACS analysis was performed to isolate GFP positive and propidium

182 iodide (PI) negative muscle cells. A fraction of PI negative cells was 'sorted' without GFP gating
183 as the "all cells" control sample. 20,000-40,000 sorting events were collected for each strain. We
184 performed four independent replicates for the wild-type and *daf-16(lf)* 'muscle cell' datasets, and
185 three independent replicates for the *daf-2(lf)* and *daf-16(lf); daf-2(lf)* 'muscle cell' datasets. RNA
186 was extracted with TRIzol, cleaned up with DNAse I, and quality checked before being sent for
187 sequencing using a protocols adapted from (Spencer et al. 2014). In parallel, aliquots of sorted
188 muscle and all cells were plated, and muscle cell enrichment was confirmed.
189
190 **Analysis of mRNA-seq data**
191 mRNA-seq raw reads were processed to produce transcript abundance and counts with Salmon
192 1.4.0. STAR and HTSeq were applied to validate estimated read maps from Salmon. Differential
193 gene expression analysis was performed with DESeq2. GraphPad Prism and Pheatmap were used
194 for visualizing abundance data.
195
196 **Analysis of ChIP-seq data**
197 ChIP-seq raw data were obtained for XE1464 (ENCFF281NRH, ENCFF657MHD,
198 ENCFF229JKH, ENCFF023XDP), ZM7247 (ENCFF004HMK, ENCFF018WCD,
199 ENCFF889RBK), and ZM8745 (ENCFF288VDV, ENCFF846OUT, ENCFF963PAM) from a
200 publicly available database (Kudron et al. 2018). To identify muscle and intestinal GFP::DAF-
201 16a binding sites, these ChIP-seq raw reads were aligned with Bowtie 2 2.4.1 and further
202 processed with SAMtools. Peaks were called with MACS2 for each replicate using the input
203 ChIP-seq data without antibody enrichment for DAF-16 binding sequences. Peaks from two
204 replicates were combined with IDR. ChIPseeker was used to identify genes that reside within 5
205 kb of the 5' or 3' of the peak, including the coding regions. ChromoMap was used to visualize
206 binding sites.
207
208 **RT-qPCR**
209 Animals were synchronized and cultured as for those used for mRNA-seq analyses. Total RNA
210 was extracted from synchronized young adult worms using TRIzol and with the method
211 described previously (Spencer et al. 2014). RT-qPCR was performed with Luna Universal One-
212 Step RT-qPCR Kit from NEB on BioRad CFX96 Touch Real-Time PCR Detection System.

213 Each RNA sample was tested with gene-specific primers (see Table S2 for sequences). We used
214 two housekeeping genes whose expression is not dependent on IIS as controls for expression.
215 *pmp-3* has been previously described (Hoogewijs et al. 2008). *rpl-17* was chosen because its
216 transcript level is high and consistent in all of our samples based on our mRNA-seq data. Each
217 RT-qPCR experiment was performed using 4 different dilutions of extracted RNA from each
218 sample. The experiment was repeated 3 times. The relative fold expression change was
219 calculated using the $2^{-\Delta\Delta CT}$ method. Specifically, at each concentration, the ΔCt between the gene
220 of interest and *rpl-17* or *pmp-3* was calculated for all genes and for all samples. At each
221 concentration, the ΔΔCt and thus fold expression change was then calculated between the wild-
222 type sample and other samples. Statistical analysis for RT-qPCR was performed by two-way
223 ANOVA with multiple comparisons between the mean of one condition with the mean of every
224 other condition followed by Šidák correction.
225
226 **Confocal fluorescent microscopy**
227 Stocks for imaging were kept at 15°C. A few adults were picked from each stock. Their first-
228 generation progenies were cultured at 20°C until L4, from which transgenic worms were picked
229 and shifted to 22.5°C (for Figure 4d, 5d, S2a, S4b) or 25°C (for Figure 4e, 4f, 5e, 6c) for one day
230 until they became young adults. Culturing conditions for dauers and starved adults in Figure S2b,
231 S2c, S3a, and S3b were as follows. For dauer experiments, worms raised at 15°C were grown at
232 25°C for at least 10 days to allow dauer formation. On the day of experiment, they were washed
233 off the plate and treated with 1% SDS for 20 minutes to select for dauers. L2/L3 larvae born and
234 raised at 15°C were used at controls in these experiments. For adult starvation experiments, ten
235 young adult worms were hand-picked onto each plate and allowed to grow at 15°C. After the
236 OP50 food was exhausted (~7 days) worms were left on the plate for another 2-3 days. Young-
237 adult-sized worms were picked for imaging. Well-fed young adults raised at 15°C were used as
238 controls. For each set of comparison applying the same transgenic line, we applied the same
239 culturing and imaging conditions and image processing procedures.
240 For imaging, live animals were placed with minimal M9 solution on dry 2% agarose pads
241 covered with a coverslip. All images were acquired using a 20x or 60x objective on a Nikon Ti2
242 spinning disk confocal microscope equipped with an Andor Zyla VSC-07720 camera, with XY
243 titled images taken with 15% overlap and Z-stacks were acquired at a step size of 2 μm (20x

244 objective) or 1 μm (60x objective). Quantification was performed with ImageJ 2.3.0 (Schindelin
245 et al. 2012) where we acquired the total and mean intensity for ROI (muscle cells, RIM) and the
246 mean intensity of a background area in the same image. To correct for background for mean
247 fluorescence, total ROI intensity was subtracted with the product of the background mean
248 intensity and the size of muscle cell; Mean ROI intensity was subtracted with the background
249 mean intensity. All images showed maximum projection. Statistical analysis for fluorescence
250 intensity was performed by two-way ANOVA with multiple comparisons between the mean of
251 one condition with the mean of every other condition followed by Šidák correction.
252
253 **Results**
254 **24 bulk mRNA-seq datasets to identify DAF-16-dependent transcriptional changes under**
255 **high and low IIS states enriched in mature body wall muscle cells**
256 To uncover muscle-enriched transcriptional changes, we started with a transgenic strain where
257 only the body wall muscle cells are labelled by GFP, which we referred to as the wild-type
258 background for mRNA-seq experiments henceforth. We used animals of four genetic
259 backgrounds, all carrying the same transgene - wild-type, *daf-16 loss-of-function (lf)* mutants,
260 *daf-2(lf)* mutants, and *daf-16(lf); daf-2(lf)* mutants (see Methods) - to model high (*daf-2(+)*) and
261 low (*daf-2(lf)*) IIS activity, with and without DAF-16 (Figure 1b). We compared DAF-16-
262 dependent transcriptional changes under the two IIS states separately.
263 Under the high IIS state, DAF-16 is maintained at the cytosol thus has low transcriptional
264 regulation activity. To obtained DAF-16-dependent transcriptional changes, we compared the
265 transcriptomes of *daf-2(+)* animals in the presence or absence of DAF-16, specifically, between
266 wild-type animals and *daf-16(lf)* mutant animals raised as synchronized cultures under optimal
267 laboratory culture conditions at 22.5°C and harvested 8 hours post the last larva molting.
268 Reduced IIS induces DAF-16's nuclear translocation and elevation of its transcriptional activity.
269 To obtain DAF-16-dependent transcriptional changes under the low IIS state, we compared the
270 transcriptome between *daf-2(lf)* single mutant and *daf-16(lf); daf-2(lf)* double mutant animals.
271 Because a full or partial functional loss of DAF-2 leads to arrest of or compromised reproductive
272 development, we raised an allele of temperature-sensitive *daf-2(lf)* larvae at the permissive
273 temperature (15°C) until they completed the last larva molt. They were further raised at the non-

274 permissive temperature (22.5°C) for 8 hours to allow accumulation of DAF-16-dependent
275 transcriptional changes (see Methods for further explanation for rationales and details).
276 To uncover muscle-enriched transcriptional changes, we dissociated these age-matched young
277 adults to collect GFP-positive cells using fluorescence-activated cell sorting (FACS) ('muscle
278 cells'; Figure 1b). Three to four replicates, each with 20,000 to 40,000 sorting events, were
279 obtained for each genotype. Control samples ('all cells'; Figure 1b) were collected after each
280 sample underwent dissociation and sorting but without GFP gating. These samples served as
281 controls not only for muscle-enriched transcripts, but also, importantly, transcriptions that reflect
282 cellular responses induced by the not-at-all subtle dissociation experimental manipulations.
283 Overall, this left us 24 samples spanning four genotypes, all with both sorted 'muscle cell' and
284 'all cell' samples. We obtained on average 45 million reads per sample (ranged from 29 to 67
285 million reads) to ensure sufficient sequencing depth. They mapped to 20,800 protein-encoding
286 genes, with at least one read in at least one dataset.
287 Our bulk assessment of the resulted sequencing datasets showed that they exhibit consistent
288 differences, in an IIS state, DAF-16 activity, and cell-type dependent manner (Figure 1c, d).
289 Principle component analyses (PCA) applied to all 24 datasets separated the 12 *daf-2(+)* samples
290 from the 12 *daf-2(lf)* samples; the latter further segregated into two clusters by the cell-type
291 ('muscle cells' versus 'all cells'), all by the first two principal components (PC) that together
292 account for 84% of the total variance (Figure 1c). Further PCA analyses, applied separately to
293 the 12 *daf-2(+)* or 12 *daf-12(lf)* samples, showed that while 12 *daf-2(+)* samples (wild-type and
294 *daf-16(lf)* samples) do not readily distinguish each other (Figure 1d, bottom panel), 12 *daf-2(lf)*
295 samples segregated into 4 distinct clusters with two PCs that account for 91% of all variance –
296 the 1st PC predominantly separates them by being either muscle cells or all cells, and the 2nd PC
297 predominantly separates them by the presence or absence of DAF-16 (Figure 1d, top panel).
298 Thus, these datasets contain sequencing information to distinguish between the high and low IIS
299 states, and at the low IIS state, DAF-16-dependent transcriptional differences both unique to
300 muscle cells and shared by all cells.
301 This evaluation warranted the subsequent application of DESeq2 analyses on these 24 datasets to
302 identify specific sets of transcriptional changes that depend on DAF-16 activation. Henceforth,
303 we refer all samples with a wild-type *daf-2* genotype (wild-type, *daf-16(lf)*) as at the high IIS
304 state, and all samples with a *daf-2(lf)* mutation (*daf-2(lf)*, and *daf-16(lf); daf-2(lf))* as at the low

305 IIS state. We refer samples both with no DAF-16 (*daf-16(lf)* and *daf-16(lf); daf-2(lf)*), and with
306 low DAF-16 activity due to high IIS (wild-type *daf-2*) as samples with 'inactive DAF-16',
307 whereas those with high DAF-16 activity, induced by low IIS (*daf-2(lf)*), as samples with 'active
308 DAF-16'.
309
310 **No prevalent DAF-16 transcriptional regulation in body wall muscle cells at high IIS state**
311 First, we compared samples at high IIS state from wild-type animals and *daf-16(lf)* mutants.
312 Consistent with a lack of distinct clustering, the DESeq2 analyses applied to 'muscle cell'
313 samples did not reveal prevalent transcript changes in the presence or absence of DAF-16
314 (Figure 2a; Table 1). Briefly, among 20,800 genes that the sequencing reads mapped to, only 11
315 passed statistical tests for differentially expressed candidates (FDR < 0.05, n = 4). Among them,
316 nine were of insufficient reads (less than 4 counts per million, CPM) in wild-type and *daf-16(lf)*
317 muscle cells; only two, *ZK105.1* and *col-33*, have >10 CPM in one genotype and none 0 CPM in
318 the other (Table 1). However, they are not among candidates at low IIS state (Figure 2b). We
319 consider them unlikely to be DAF-16 targets. This negative outcome corroborates conclusions
320 from previous mRNA-seq analyses applied to samples prepared from intact animals: there were
321 no appreciable transcriptional differences between wild-type animals and *daf-16(lf)* mutants
322 under normal culture conditions (Hibshman et al. 2017; Li et al. 2019).
323 For our study, this outcome, which contrasts that at the low IIS state (below), born another
324 critical significance. Because the dissociation and FACS-sorting process imposed acute cellular
325 stress regardless of the genotype, this negative outcome showed that our experimental paradigm
326 was able to maintain DAF-16 activity sufficiently low under normal growth conditions, and our
327 analysis pipeline is sufficiently robust against noises induced by experimental manipulation.
328 In summary, we confirm that DAF-16's transcriptional activity is low in muscle cells, where
329 normal culture conditions maintain IIS at the high state.
330
331 **195 candidates for DAF-16 regulation in body wall muscle cells at low IIS state**
332 In contrast to samples at the high IIS state, and consistent with their distinct clustering, our
333 DESeq2 analyses of the 'muscle cells' at the low IIS state revealed a substantial number of
334 candidate DAF-16 targets. Transcript levels from 312 genes showed statistically significant
335 differences between the *daf-2(lf)* and *daf-16(lf); daf-2(lf)* samples (FDR < 0.05, n = 3), 142 being

336 upregulated and 170 being downregulated. This list warrants a further evaluation of DAF-16-
337 dependent transcriptional regulation.
338 To identify the most consistent transcriptional changes induced by DAF-16 activation, we
339 filtered this list against two more sets of transcriptomes with inactive DAF-16. Specifically, after
340 we compared *daf-2(lf)* against wild-type, *daf-16(lf)* and *daf-16(lf); daf-2(lf)* 'muscle cell'
341 samples, we kept those that showed statistical differences in all three comparisons. We reason
342 that this step helps to reduce noise that may rise from stochastic compensation for a constitutive
343 DAF-16 loss, and from the small number of replicates per genotype.
344 This leaves us 195 candidates - 88 upregulated and 107 downregulated - upon DAF-16 activation
345 (Table 2; Table S3).
346
347 **139 candidates for body muscle cell-enriched DAF-16 regulation under a low IIS state**
348 Among this list we sought candidates that are selectively regulated by DAF-16 in the body wall
349 muscle cells. First, we compared the abundance of 195 candidates in active DAF-16 samples
350 (*daf-2(lf))* that were sorted ('muscle cells') or not sorted ('all cells'), and filtered 43 that
351 exhibited similar abundances. Remaining 152 genes with either enrichment or depletion in
352 muscle cells were further compared to two more sets of transcriptomes with inactive DAF-16
353 (wild-type and *daf-16(lf)*) from 'all cells'. This resulted in a list of 139 genes (62 upregulated and
354 77 downregulated) to be preferentially affected by DAF-16 in body wall muscle cells (Figure 2c;
355 Table 2; Table S4).
356 While a transcriptional regulation event shared by muscle and non-muscle cells does not exclude
357 a muscle-specific function, we chose to focus on a smaller candidate list to further evaluate their
358 candidacy as muscle-specific DAF-16 targets.
359
360 **12 candidate DAF-16 muscle-specific targets under a low IIS state**
361 Transcription factors affect a transcriptome directly, by binding the regulatory elements of a gene
362 that leads to its activation or repression, as well as indirectly, such as by its primary targets
363 modulating transcription in various ways. We sought DAF-16's primary transcriptional targets
364 by considering DAF-16-binding sites revealed by tissue-specific ChIP-seq analyses.
365 We previously generated a set of *daf-16(lf); daf-2(lf)* strains that each carry a single-copy
366 transgene that expresses, from the same genomic locus, functional GFP::DAF-16a from the

367 intestine cells or the muscle cells (Hung et al. 2014). They were used to generate the bulk of
368 publicly available GFP::DAF-16a-ChIP-seq reads (Kudron et al. 2018). We previously chose the
369 DAF-16a isoform because this, not the other (b, d/f) isoforms, was required in muscle cells for
370 neuromuscular junction maturation (Hung et al. 2013). From these reads, we mapped 1,919
371 binding sites in the muscle-specific GFP::DAF-16a strain, and 955 and 2,422 binding sites in two
372 independently derived intestine-specific GFP::DAF-16a strains (Table S5). ChIP-seq read peaks
373 spanned widely across all six chromosomes (Figure 3a), consistent with the previous assessment
374 that only a small fraction of DAF-16 binding events lead to transcriptional activation (Schuster et
375 al. 2010).
376 Among the 139 DAF-16 candidate targets, 55 showed at least one GFP::DAF-16a binding site
377 within its genomic locus that begins at 5kb upstream of the first predicted or confirmed
378 translational start site and ends at 5 kb downstream of the first predicted or confirmed stop
379 codon. 43 are upregulated and 12 are downregulated by activated DAF-16 (Figure 3b; Table S6).
380 Among them, 14 have the GFP::DAF-16a binding present in the muscle ChIP-seq dataset, but
381 absent in both intestine ChIP-seq datasets. Removing those with low reads, we are left with 12
382 candidates, all being upregulated by activated DAF-16a (Figure 3b; Table 3).
383 Overall, this workflow applies progressively stringent criteria to narrow the candidacy of DAF-
384 16 primary targets from an initially large list of transcriptional differences between the muscle
385 cells harvested from *daf-2(lf)* and *daf-16(lf); daf-2(lf)* animals (Figure 3c: Table 2). Due to the
386 limited number of replicates of mRNA-seq samples, insufficient replicates of ChIP-seq datasets
387 as well as lack of raw reads of other tissue-specific ChIP-seq datasets, we took orthogonal
388 approaches, described in Sections below, to further verify the candidacy of selected muscle-
389 specific DAF-16 regulation.
390
391 **Validation of selected candidates with mRNA samples from non-transgenic strains**
392 We ordered the 12 candidates, first by their fold changes between muscle samples with or
393 without DAF-16 under a low IIS state, followed by their relative abundance (Table 3). Four top
394 candidates are *C54F6.5*, *cex-1*, *gstk-2* and *mlcd-1*. Among them, all but *gstk-2* possess at least
395 one DAF-16 binding element (DBE), a consensus DAF-16-binding cassette previously
396 implicated in transcriptional regulation (Murphy et al. 2003; Schuster et al. 2010; Tepper et al.
397 2013), within or at the vicinity of identified DAF-16a binding sites (Figures 4c, 5c, 6b, S4b). All

398 are ranked low for DAF-16-dependent transcriptional changes from whole-animal studies
399 (Tepper et al. 2013).
400 Because our mRNA-seq datasets were obtained from dissociated cells, we wanted to first verify
401 some candidates using RNA samples independently prepared from intact *C. elegans* samples and
402 strains without transgenic markers. Using total mRNA prepared from synchronized and age-
403 matched, non-transgenic wild-type (N2), *daf-2(lf)*, *daf-16(lf)*, and *daf-16(lf); daf-2(lf)* young
404 adults, cultured in conditions similar to that of cell-sorting mRNA-seq experiments, we
405 quantified the transcript level using RT-qPCR. We reason that upregulation of two high-
406 abundance and high-fold change candidates, *C54F6.5* or *cex-1*, are the most likely be detectable
407 in total RNA. Indeed, an upregulation of *C54F6.5* transcripts was also notable between our *daf-*
408 *2(lf)* and *daf-16(lf); daf-2(lf)* 'all cells' samples (Figure 4a).
409 Our RT-qPCR analyses recapitulated DAF-16-dependent upregulation of *C54F6.5* and *cex-1*
410 transcripts in *daf-2(lf)* mutants (Figure S1; Figure 4b; Figure 5b). Consistent with their rank, the
411 transcript level of *C54F6.5* was the more robustly upregulated in active DAF-16 samples, similar
412 to that of *sod-3*, a known pan-tissue DAF-16 target (Figure S1).
413
414 **DAF-16 upregulates multiple reporters for C54F6.5 in body wall muscle cells**
415 *C54F6.5* is predicted (Blum et al. 2021) to encode a secreted 56-amino acid protein without
416 functional characterization. With close to 0 read in all inactive DAF-16 muscle samples and high
417 fold changes in active DAF-16 samples (Figure 4a; Figure 4b), we further examined its
418 regulation with both transcriptional and translational reporters.
419 Immediately upstream of *C54F6.5* coding region resides a DAF-16a-ChIP-seq peak with DBE
420 that is present only in the muscle datasets (Figure 4c, top panel). Several reporters with promoter
421 sequences consisted of this region (Figure 4c, bottom panels; Methods) exhibited DAF-16-
422 dependent, robust expression in body wall muscle cells or nuclei (Figure 4d-e, BWM) and DAF-
423 16-independent expression in a non-muscle tissue, spermatheca (Figure 4d-e, SP). Consistent
424 with *C54F6.5* being a secreted protein, translational reporters, where the full *C54F6.5* coding
425 sequence fused with GFP, accumulated fluorescent signals in coelomocytes (Figure S2a), the
426 scavenger cells that collect proteins in the body fluid (Fares and Greenwald 2001).
427 In body wall muscle cells, in the presence of DAF-16, both transcriptional reporters - one with
428 endogenous 3' UTR and another with a generic 3' transcriptional enhancer - showed sporadic

429 and weak signal in high IIS state (wild-type animals), but consistent and robust signals in low IIS
430 state (*daf-2(lf)* mutant animals). Both sets of signals were eliminated by the absence of DAF-16
431 (*daf-16(lf)* and *daf-16(lf); daf-2(lf)*) (Figure 4d-f). Multiple lines of analyses thus consistently
432 support the notion of a muscle cell-specific IIS regulation of *C54F6.5*.
433

434 **DAF-16 upregulates reporters for CEX-1/Calexcitin, a Ca^{2+} binding protein, in body wall**
435 **muscle cells**

436 CEX-1 is the *C. elegans* homologue of Calexcitin, a Ca^{2+} binding protein. *cex-1* exhibits low
437 reads in inactive DAF-16 'muscle cells', and high fold read increases in active DAF-16 samples
438 (Figure 4a). Further verification of *cex-1* as a top candidate DAF-16 target by RT-qPCR (Figure
439 4b) was initially a surprise, because a *cex-1* promoter has long been used to drive constitutive
440 gene expression in a single pair of interneuron (RIM) (Cohen et al. 2009; De Rosa et al. 2019).
441 Our ChIP-seq analyses revealed a DAF-16a binding site with DBE at the 3' UTR of *cex-1* that
442 was only occupied in the muscle dataset (Figure 5c). Upon including *cex-1* 3' UTR fragment
443 with this site, a *cex-1* transcriptional reporter exhibited an expression pattern that corroborates
444 the mRNA-seq and ChIP-seq results: a DAF-16-dependent upregulated expression in muscle
445 cells (Figure 5d, BWM), and a DAF-16-independent constitutive expression in the RIM neuron
446 (Figure 5d, RIM) and pharyngeal muscles (Figure 5d, PM). Consistent signals across four
447 genotypes in RIM soma (Figure 5d, right panel) corroborated with a higher *cex-1* read counts in
448 the 'all cells' samples by DAF-16-independent transcription activation.
449 Lastly, a *rfp::cex-1* translational reporter expressed from the endogenous genomic locus (Figure
450 5c) showed robust expression in the RIM neuron (Figure 5e, RIM), and low expression in body
451 wall muscles comparable between wildtype, *daf-16(lf)*, and *daf-16(lf); daf-2(lf)* young adults
452 (Figure 5e, BWM). DAF-16-dependent *rfp::cex-1* upregulation was observed in the body wall
453 muscle cells of *daf-2(lf)* young adults (Figure 5e, *daf-2* panel, right panel). These results are
454 consistent with a DAF-16-dependent *cex-1* transcriptional regulation specific for the body wall
455 muscles and more prominent in low IIS state.
456

457 **DAF-16 upregulates a reporter for MLCD-1/MCD, a malonyl-CoA decarboxylase, in body**
458 **wall muscle cells**

459 *mlcd-1* encodes a fatty acid metabolic enzyme, malonyl-CoA decarboxylase (MCD). Ite
460 exhibited overall lower transcript abundance than the other two candidates, but high fold changes
461 (Figure 6a). A transcriptional reporter that consists of *mlcd-1* 5' sequence with a DBE region and
462 3' UTR (Figure 6b) showed body wall muscle-specific expression in *daf-2(lf)* young adults
463 (Figure 6c, *daf-2* panel, BWM). The same transgene showed little signals in wild-type, *daf-16(lf)*
464 and *daf-16(lf); daf-2(lf)* animals (Figure 6c). In our study, this reporter showed not only strong
465 DAF-16-dependent expression, but also the highest specificity for body wall muscle cells.
466
467 ***C54F6.5*, *cex-1*, and *mlcd-1* reporter expression was altered in body wall muscle cells by**
468 **physiological processes regulated by IIS**
469 DAF-16 targets are likely to alter their expression in physiological states regulated by IIS. We
470 qualitatively assessed how above reporters responded under two such physiological states, dauer
471 formation and adult starvation.
472 For juvenile larvae, environmental stress such as food deprivation at high population density,
473 triggers them to halt reproductive development and to enter dauer diapause (Fielenbach and
474 Antebi 2008). This transition requires DAF-2-regulated transcriptional activation across tissues,
475 and *daf-2(lf)* larvae activate dauer diapause even without food deprivation. We found that wild-
476 type dauers (induced by poor environment), as well as *daf-2(lf)* dauers (induced by juvenile
477 larvae at non-permissive temperatures), reporters for *C54F6.5* (Figure S2b and S2c, left panels),
478 *cex-1* (Figure S3a, left panels), and *mlcd-1* (Figure S3b; left panels) all showed potent activation
479 in body wall muscles BWM in Figure S2 and S3). The *cex-1* reporter was further activated in
480 enteric muscles (AS, AD in Figure S3a, left panels).
481 Their responses to adult starvation, for which we surveyed both wildtype adults and *daf-2* adults
482 raised at permissive temperature, showed a similar trend but less robust and consistent than in the
483 dauer larvae. For example, while both *C54F6.5* transcriptional (Figure S2b, right panels) and
484 translational reporters (Figure S2c, right panels) were activated in the body wall muscles of
485 starved adults in comparison to fed adults, the transcriptional reporter exhibited a more
486 prominent response and in starved *daf-2* adults. The *mlcd-1* transcriptional reporter similarly
487 showed activation in both starved adults, but more prominently in *daf-2* adults (Figure S3b, right
488 panels). The *cex-1* translational reporter showed the least response in starved adults (Figure S3b,
489 right panels) when compared to dauer larvae (Figure S3b, left panels).

490 These qualitative assessment, especially the reporter's activation in dauer larvae lends further
491 support that these genes likely represent bona fide DAF-16 targets in body wall muscles.
492
493 **Ambiguity of remaining candidates**
494 We consider the candidacy of all remaining genes to be low, because of their low reads, or a
495 moderate fold change for transcripts with high or moderate reads (Table 3). We tested *gstk-2*,
496 which ranked the highest among them (Table 3; Figure S4a), with an endogenous GFP reporter.
497 Specifically, a cassette of splice leader 2 (*sl2*)-*gfp* inserted into the *gstk-2* locus drove co-
498 transcription but separate translation of GSTK-2 and GFP (Figure S4b). It showed GFP
499 expression in body wall muscles (BWM), pharynx cells (PH), and epithelial seam cells (SC)
500 across wild-type, *daf-16(lf), daf-2(lf)*, and *daf-16(lf); daf-2(lf)* animals, without obvious
501 differences in fluorescent intensity (Figure S4b). While we do not exclude experimental fallacies
502 such as higher stability of the GFP reporter itself masking moderate differences at the protein
503 level, we did not proceed further with this and remaining candidates.
504
505 **Discussion**
506 A limited number of signaling pathways regulate numerous and diverse developmental processes
507 in an organism- and cell-type-specific manner. IIS exerts physiological functions with tissue- and
508 cell-specificity, and with both cell-autonomy and non-autonomy. Applying a rigorous workflow
509 that reveals three new DAF-16 targets in body wall muscle cells, we contribute understanding
510 towards the intricacy and mechanism of tissue-specific function exerted by a molecularly
511 conserved and ubiquitously active signaling pathway.
512
513 **A small yield for tissue-specific DAF-16 targets**
514 Combining mRNA-seq, ChIP-seq, RT-qPCR, and reporter analyses, we report three high-
515 confidence DAF-16 targets primarily in the body wall muscle cells. Here we applied a series of
516 increasingly stringent bioinformatic criteria that led to a small list of muscle-specific DAF-16
517 transcriptional targets (Figure 3c; Table 2). Reporter analyses for three of the four top candidates,
518 all being overlooked in previous whole animal studies, lends support to this stringent approach.
519 Both negative and positive outcome from these analyses provided a few empirical guides to filter
520 and enrich for differential gene expression events of physiological significance to follow

521 through. Three targets constitute a minuscule fraction of the 139 genes that showed DAF-16-
522 dependent, muscle-enriched transcript changes. We do not know how many primary DAF-16
523 targets drive the broader state of transcriptional changes, but we expected a lower representation
524 of the primary transcriptional target, because a full transcriptome reflects the physiological state
525 of cells.
526 However, this extremely low yield deserves further scrutiny, as described below.
527
528 **Limitation of this stringent approach**
529 Our final candidate list (12 genes) is small, and three validated genes covered all high-
530 confidence ones on the list. At this time, we do not know whether this short list reflects true
531 physiology of muscle cells, where only a handful of molecular drivers underlie muscle-unique
532 IIS regulation, or, high false negatives, where our stringent criteria led to excessive exclusion of
533 DAF-16 transcriptional targets with functional relevance to muscle cells. Empirically, we favor
534 the second possibility for several reasons.
535 First, by requiring both muscle-specific DAF-16 transcription regulation and muscle-enriched
536 DAF-16a binding, we have biased against genes playing critical physiological functions at fast
537 temporal dynamics or at low abundance.
538 Second, we have no criteria to objectively evaluate the coverage and consistency of the ChIP-seq
539 reads. We noted that our sequential filtering during muscle-enriched transcriptomics analyses
540 have maintained many high-confidence DAF-16 targets previously identified in whole-animal
541 studies (Murphy et al. 2003; Tepper et al. 2013; Kaletsky et al. 2016) (Table S3, S4, S6), but
542 many such candidates were removed when we applied the muscle ChIP-seq dataset as the first
543 filter (Figure 3b, c). More specifically, imposing the presence of a binding site of muscle
544 GFP::DAF-16a led to removal of ~2/3 of candidates, which includes *sod-3*, a gold standard of
545 the field and our positive control for RT-qPCR analyses (Figure S1). This raised concerns for
546 missing targets due to the available muscle ChIP-seq reads.
547 Exclusion of isoforms other than DAF-16a in the ChIP-seq experiments may account for this
548 concern; it is also possible that both muscle and intestine DAF-16 ChIP-seq experiments, being
549 carried out as part of a systematic survey for transcription factors, were not as tightly controlled
550 for developmental stages or genome coverage (Kudron et al. 2018), as for the focused mRNA-
551 seq effort. Lastly, although we already broadened the region for gene mapping near the DAF-16a

552 binding sites than regions considered for enrichment of the DBE sites in previous studies,
553 regions to be explored remains an arbitrary criterion.
554
555 **Potential physiological functions of three DAF-16 targets**
556 Physiological functions of three newly identified muscle DAF-16 targets are currently unknown,
557 but we make a few speculations.
558 C54F6.5 is a small secreted protein. It has no apparent homolog outside the nematode specie by
559 primary sequence alignment; however, we do not have reliable mean to predict structural
560 similarity among small secreted proteins. Indeed, while amino acid sequences for many *C.*
561 *elegans* neuropeptides revealed poor homologies, thus deemed to be 'nematode-specific', several
562 have been shown to activate evolutionarily conserved GPCR signaling and to serve homologous
563 physiological functions (Li 2008 Sep 25; Chen et al. 2022). C54F6.5 is one of many small
564 secreted 'nematode-specific' proteins. These proteins are enriched for regulation upon exposure
565 to pathogens and have been proposed to underlie the *C. elegans* immune response (Suh and
566 Hutter 2012; Zhao et al. 2021). C54F6.5 might constitute a component of defense mechanisms
567 contributed by muscle cells.
568 CEX-1 is homologous to calexcitin, a proposed Ca^{2+} sensor that regulates neuronal activity for
569 learning (Nelson et al. 1996; Alkon et al. 1998; Nelson et al. 1999). With three Ca^{2+}-binding EF-
570 hand domains, it allows the cell to modulate its membrane excitability via the K^+ channel and
571 ryanodine receptor in a Ca^{2+}-dependent manner (Alkon et al. 1998). Consistently, calexcitin was
572 shown to bind ryanodine receptors in the sarcoplasmic reticulum (Gombos et al. 2001). In *C.*
573 *elegans*, a bit ironically, there has been no functional studies on the *cex-1* gene itself, despite a
574 fragment of its promoter being a popular tool to manipulate RIM, a neuron involved in
575 associative learning, decision-making (Gordus et al. 2015; Jin et al. 2016; Sordillo and
576 Bargmann 2021), and neuronal activation-induced stress response (De Rosa et al. 2019). CEX-
577 1's muscle up-regulation by DAF-16 promotes several hypotheses, for example, contribution to
578 DAF-16-dependent effects on calcium homeostasis, motility, and health (Oh and Kim 2013; Roy
579 et al. 2022; Momma et al. 2017).
580 MLCD-1, the *C. elegans* malonyl CoA decarboxylase (MCD) offers the clearest functional
581 implication. MCD is abundantly expressed in the heart and skeletal muscles. Malonyl CoA is a
582 potent inhibitor of carnitine palmitoyltransferase, an enzyme that transports long chain fatty acid

583 into the mitochondria for ATP production. By breaking down malonyl CoA, MCD mobilizes
584 fatty acid-driven energy production. Unlike the other two targets, the *mlcd-1* reporter is activated
585 only in body wall muscles. Previous whole-animal RNA-seq datasets identified *mlcd-1* and other
586 fatty acid metabolic enzyme-encoding genes to be upregulated by DAF-16 in context of
587 longevity (Amrit et al. 2016), but our 139 muscle-enriched candidate DAF-16 targets do not
588 include these other enzymes. MLCD-1 might modify the balance of energy storage and
589 expenditure, instead of (or at least in addition to) simply boosting fatty acid oxidation in body
590 wall muscle cells.
591 Muscle energy mobilization is particularly important for metabolism. We further speculate that
592 DAF-16's targeting of both CEX-1 and MCD-1 in muscle cells may reflect an orchestrated effort
593 to increase muscle function as part of shared responses induced by reduced IIS signaling.
594
595 **Future directions**
596 Future studies should address physiological functions of C54F6.5, CEX-1, and MLCD-1 in
597 context of IIS signaling-related developmental and physiological processes. As mentioned in
598 previous sections, behavioral and physiological consequences of single or combined knockout of
599 these target genes, such as pathogen resistance, motility, and muscle physiology, under low and
600 high IIS states serves as an excellent starting point. A requirement of either gene in respective
601 phenotypes of *daf-2(lf)* mutants can then be further examined by standard molecular genetic
602 manipulation, such as tissue-specific rescue or deletion.
603 Future studies should evaluate the validity of applying the ChIP-seq data to filter direct targets of
604 transcription factors. This means that our 139 candidates from the mRNA-seq analyses should be
605 independently evaluated for DAF-16-dependent transcriptional regulation. Ideally, a systematic,
606 endogenous genomic tagging of these genes provides the needed assessment of required quality
607 and coverage to incorporate information from future ChIP-seq datasets in search for cell-type
608 specific and direct targets.

Data Availability Statement Strains underlined in Table S1, plasmids underlined in Table S1, and mRNA-sequencing data are available at CGC, Addgene, and GEO (GSE315486), respectively.

Acknowledgments We thank Kin Chan of the Network Biology Collaborative Centre Next-Generation Sequencing Facility (RRID: SCR_025385) at the Lunenfeld-Tanenbaum Research Institute for mRNA-seq. The facility is supported by the Canada Foundation for Innovation and the Ontario Government. We thank Arneet Saltzman and Tammy Lee for advice on mRNA-seq, ChIP-seq, and RT-qPCR. We acknowledge NIH support for CGC, where we deposited strains for distribution. We acknowledge WormBase (Sternberg et al. 2024) for support.

Funding Natural Sciences and Engineering Research Council of Canada RGPIN-2017-06738 (to M.Z.) and USRA (to S.W.).

Author contributions M.Z. conceptualization; M.Z., W.H. supervision; S.W., J.G., W.H. experimental design, data collection and analyses; Y.L., C.R., Y.W., S.R., B.M., W.L., J.C. reagents and data collection; S.W., J.G. visualization; S.W., W.H., M.Z manuscript drafts; B.M. editing; M.Z. funding.

627 **Literature Cited**

628 Aghayeva U, Bhattacharya A, Sural S, Jaeger E, Churgin M, Fang-Yen C, Hobert O. 2021.
629 DAF-16/FoxO and DAF-12/VDR control cellular plasticity both cell-autonomously and via
630 interorgan signaling. PLoS Biol. 19(4):e3001204. doi:10.1371/journal.pbio.3001204.

631 Alkon DL, Nelson TJ, Zhao W, Cavallaro S. 1998. Time domains of neuronal Ca2+ signaling
632 and associative memory: steps through a calexcitin, ryanodine receptor, K+ channel cascade.
633 Trends Neurosci. 21(12):529–537. doi:10.1016/s0166-2236(98)01277-6.

634 Amrit FRG, Steenkiste EM, Ratnappan R, Chen S-W, McClendon TB, Kostka D, Yanowitz J,
635 Olsen CP, Ghazi A. 2016. DAF-16 and TCER-1 Facilitate Adaptation to Germline Loss by
636 Restoring Lipid Homeostasis and Repressing Reproductive Physiology in C. elegans. PLoS
637 Genet. 12(2):e1005788. doi:10.1371/journal.pgen.1005788.

638 Blum M, Chang H-Y, Chuguransky S, Grego T, Kandasaamy S, Mitchell A, Nuka G, Paysan-
639 Lafosse T, Qureshi M, Raj S, et al. 2021. The InterPro protein families and domains database: 20
640 years on. Nucleic Acids Res. 49(D1):D344–D354. doi:10.1093/nar/gkaa977.

641 Brenner S. 1974. The genetics of Caenorhabditis elegans. Genetics. 77(1):71–94.
642 doi:10.1093/genetics/77.1.71.

643 Byrne AB, Walradt T, Gardner KE, Hubbert A, Reinke V, Hammarlund M. 2014. Insulin/IGF1
644 Signaling Inhibits Age-Dependent Axon Regeneration. Neuron. 81(3):561–573.
645 doi:10.1016/j.neuron.2013.11.019.

646 Chen L, Liu Y, Su P, Hung W, Li H, Wang Y, Yue Z, Ge M-H, Wu Z-X, Zhang Y, et al. 2022.
647 Escape steering by cholecystokinin peptidergic signaling. Cell Rep. 38(6):110330.
648 doi:10.1016/j.celrep.2022.110330.

649 Chen Z, Hendricks M, Cornils A, Maier W, Alcedo J, Zhang Y. 2013. Two insulin-like peptides
650 antagonistically regulate aversive olfactory learning in C. elegans. Neuron. 77(3):572–585.
651 doi:10.1016/j.neuron.2012.11.025.

652 Chiu S-L, Cline HT. 2010. Insulin receptor signaling in the development of neuronal structure
653 and function. Neural Develop. 5:7. doi:10.1186/1749-8104-5-7.

654 Cohen M, Reale V, Olofsson B, Knights A, Evans P, de Bono M. 2009. Coordinated regulation
655 of foraging and metabolism in C. elegans by RFamide neuropeptide signaling. Cell Metab.
656 9(4):375–385. doi:10.1016/j.cmet.2009.02.003.

657 De Rosa MJ, Veuthey T, Florman J, Grant J, Blanco MG, Andersen N, Donnelly J, Rayes D,
658 Alkema MJ. 2019. The flight response impairs cytoprotective mechanisms by activating the
659 insulin pathway. Nature. 573(7772):135–138. doi:10.1038/s41586-019-1524-5.

660 Dixon SJ, Alexander M, Chan KKM, Roy PJ. 2008. Insulin-like signaling negatively regulates
661 muscle arm extension through DAF-12 in Caenorhabditis elegans. Dev Biol. 318(1):153–161.
662 doi:10.1016/j.ydbio.2008.03.019.

663 Fares H, Greenwald I. 2001. Genetic Analysis of Endocytosis in Caenorhabditis elegans:
664 Coelomocyte Uptake Defective Mutants. Genetics. 159(1):133–145.
665 doi:10.1093/genetics/159.1.133.

666 Fernandes de Abreu DA, Caballero A, Fardel P, Stroustrup N, Chen Z, Lee K, Keyes WD, Nash
667 ZM, López-Moyado IF, Vaggi F, et al. 2014. An insulin-to-insulin regulatory network
668 orchestrates phenotypic specificity in development and physiology. PLoS Genet.
669 10(3):e1004225. doi:10.1371/journal.pgen.1004225.

670 Fielenbach N, Antebi A. 2008. C. elegans dauer formation and the molecular basis of plasticity.
671 Genes Dev. 22(16):2149–2165. doi:10.1101/gad.1701508.

672 Gombos Z, Jeromin A, Mal TK, Chakrabartty A, Ikura M. 2001. Calexcitin B Is a New Member
673 of the Sarcoplasmic Calcium-binding Protein Family. J Biol Chem. 276(25):22529–22536.
674 doi:10.1074/jbc.M010508200.

675 Gordus A, Pokala N, Levy S, Flavell SW, Bargmann CI. 2015. Feedback from network states
676 generates variability in a probabilistic olfactory circuit. Cell. 161(2):215–227.
677 doi:10.1016/j.cell.2015.02.018.

678 Gottlieb S, Ruvkun G. 1994. daf-2, daf-16 and daf-23: genetically interacting genes controlling
679 Dauer formation in Caenorhabditis elegans. Genetics. 137(1):107–120.
680 doi:10.1093/genetics/137.1.107.

681 Hahm J-H, Kim S, DiLoreto R, Shi C, Lee S-JV, Murphy CT, Nam HG. 2015. C. elegans
682 maximum velocity correlates with healthspan and is maintained in worms with an insulin
683 receptor mutation. Nat Commun. 6:8919. doi:10.1038/ncomms9919.

684 Henderson ST, Johnson TE. 2001. daf-16 integrates developmental and environmental inputs to
685 mediate aging in the nematode Caenorhabditis elegans. Curr Biol CB. 11(24):1975–1980.
686 doi:10.1016/s0960-9822(01)00594-2.

687 Hibshman JD, Doan AE, Moore BT, Kaplan RE, Hung A, Webster AK, Bhatt DP, Chitrakar R,
688 Hirschey MD, Baugh LR. 2017. daf-16/FoxO promotes gluconeogenesis and trehalose synthesis
689 during starvation to support survival. eLife. 6:e30057. doi:10.7554/eLife.30057.

690 Hoogewijs D, Houthoofd K, Matthijssens F, Vandesompele J, Vanfleteren JR. 2008. Selection
691 and validation of a set of reliable reference genes for quantitative sod gene expression analysis in
692 C. elegans. BMC Mol Biol. 9(1):9. doi:10.1186/1471-2199-9-9.

693 Hung WL, Hwang C, Gao S, Liao EH, Chitturi J, Wang Y, Li H, Stigloher C, Bessereau J-L,
694 Zhen M. 2013. Attenuation of insulin signalling contributes to FSN-1-mediated regulation of
695 synapse development. EMBO J. 32(12):1745–1760. doi:10.1038/emboj.2013.91.

696 Hung WL, Wang Y, Chitturi J, Zhen M. 2014. A *Caenorhabditis elegans* developmental
697 decision requires insulin signaling-mediated neuron-intestine communication. Development.
698 141(8):1767–1779. doi:10.1242/dev.103846.

699 Ji N, Venkatachalam V, Rodgers HD, Hung W, Kawano T, Clark CM, Lim M, Alkema MJ,
700 Zhen M, Samuel AD. 2021. Corollary discharge promotes a sustained motor state in a neural
701 circuit for navigation. Zimmer M, Calabrese RL, editors. eLife. 10:e68848.
702 doi:10.7554/eLife.68848.

703 Jin X, Pokala N, Bargmann CI. 2016. Distinct Circuits for the Formation and Retrieval of an
704 Imprinted Olfactory Memory. Cell. 164(4):632–643. doi:10.1016/j.cell.2016.01.007.

705 Kaletsky R, Lakhina V, Arey R, Williams A, Landis J, Ashraf J, Murphy CT. 2016. The C.
706 elegans adult neuronal IIS/FOXO transcriptome reveals adult phenotype regulators. Nature.
707 529(7584):92–96. doi:10.1038/nature16483.

708 Kaletsky R, Murphy CT. 2010. The role of insulin/IGF-like signaling in C. elegans longevity and
709 aging. Dis Model Mech. 3(7–8):415–419. doi:10.1242/dmm.001040.

710 Kaplan REW, Chen Y, Moore BT, Jordan JM, Maxwell CS, Schindler AJ, Baugh LR. 2015. dbl-
711 1/TGF-β and daf-12/NHR Signaling Mediate Cell-Nonautonomous Effects of daf-16/FOXO on
712 Starvation-Induced Developmental Arrest. Ashrafi K, editor. PLOS Genet. 11(12):e1005731.
713 doi:10.1371/journal.pgen.1005731.

714 Kenyon C, Chang J, Gensch E, Rudner A, Tabtiang R. 1993. A C. elegans mutant that lives
715 twice as long as wild type. Nature. 366(6454):461–464. doi:10.1038/366461a0.

716 Kenyon CJ. 2010. The genetics of ageing. Nature. 464(7288):504–512.
717 doi:10.1038/nature08980.

718 Kimura KD, Tissenbaum HA, Liu Y, Ruvkun G. 1997. daf-2, an insulin receptor-like gene that
719 regulates longevity and diapause in Caenorhabditis elegans. Science. 277(5328):942–946.
720 doi:10.1126/science.277.5328.942.

721 Kleemann GA, Murphy CT. 2009. The endocrine regulation of aging in Caenorhabditis elegans.
722 Mol Cell Endocrinol. 299(1):51–57. doi:10.1016/j.mce.2008.10.048.

723 Klöckener T, Hess S, Belgardt BF, Paeger L, Verhagen LAW, Husch A, Sohn J-W, Hampel B,
724 Dhillon H, Zigman JM, et al. 2011. High-fat feeding promotes obesity via insulin receptor/PI3K-
725 dependent inhibition of SF-1 VMH neurons. Nat Neurosci. 14(7):911–918. doi:10.1038/nn.2847.

726 Kodama E, Kuhara A, Mohri-Shiomi A, Kimura KD, Okumura M, Tomioka M, Iino Y, Mori I.
727 2006. Insulin-like signaling and the neural circuit for integrative behavior in C. elegans. Genes
728 Dev. 20(21):2955–2960. doi:10.1101/gad.1479906.

729 Kudron MM, Victorsen A, Gevirtzman L, Hillier LW, Fisher WW, Vafeados D, Kirkey M,
730 Hammonds AS, Gersch J, Ammouri H, et al. 2018. The ModERN Resource: Genome-Wide
731 Binding Profiles for Hundreds of Drosophila and Caenorhabditis elegans Transcription Factors.
732 Genetics. 208(3):937–949. doi:10.1534/genetics.117.300657.

733 Lee RY, Hench J, Ruvkun G. 2001. Regulation of C. elegans DAF-16 and its human ortholog
734 FKHRL1 by the daf-2 insulin-like signaling pathway. Curr Biol CB. 11(24):1950–1957.
735 doi:10.1016/s0960-9822(01)00595-4.

736 Lee S-J, Murphy CT, Kenyon C. 2009. Glucose Shortens the Life Span of C. elegans by
737 Downregulating DAF-16/FOXO Activity and Aquaporin Gene Expression. Cell Metab.
738 10(5):379–391. doi:10.1016/j.cmet.2009.10.003.

739 Li C. 2008 Sep 25. Neuropeptides. WormBook.:1–36. doi:10.1895/wormbook.1.142.1.

740 Li S, Zhao H, Zhang P, Liang C, Zhang Y, Hsu A, Dong M. 2019. DAF-16 stabilizes the aging
741 transcriptome and is activated in mid-aged Caenorhabditis elegans to cope with internal stress.
742 Aging Cell. 18(3):e12896. doi:10.1111/acel.12896.

743 Li W, Kennedy SG, Ruvkun G. 2003. daf-28 encodes a C. elegans insulin superfamily member
744 that is regulated by environmental cues and acts in the DAF-2 signaling pathway. Genes Dev.
745 17(7):844–858. doi:10.1101/gad.1066503.

746 Libina N, Berman JR, Kenyon C. 2003. Tissue-Specific Activities of C. elegans DAF-16 in the
747 Regulation of Lifespan. Cell. 115(4):489–502. doi:10.1016/S0092-8674(03)00889-4.

748 Lin CHA, Tomioka M, Pereira S, Sellings L, Iino Y, van der Kooy D. 2010. Insulin signaling
749 plays a dual role in Caenorhabditis elegans memory acquisition and memory retrieval. J Neurosci
750 Off J Soc Neurosci. 30(23):8001–8011. doi:10.1523/JNEUROSCI.4636-09.2010.

751 Liu J, Visser-Grieve S, Boudreau J, Yeung B, Lo S, Chamberlain G, Yu F, Sun T, Papanicolaou
752 T, Lam A, et al. 2014. Insulin activates the insulin receptor to downregulate the PTEN tumour
753 suppressor. Oncogene. 33(29):3878–3885. doi:10.1038/onc.2013.347.

754 Liu Jie, Zhang B, Lei H, Feng Z, Liu Jianfeng, Hsu A-L, Xu XZS. 2013. Functional aging in the
755 nervous system contributes to age-dependent motor activity decline in C. elegans. Cell Metab.
756 18(3):392–402. doi:10.1016/j.cmet.2013.08.007.

757 Man HY, Lin JW, Ju WH, Ahmadian G, Liu L, Becker LE, Sheng M, Wang YT. 2000.
758 Regulation of AMPA receptor-mediated synaptic transmission by clathrin-dependent receptor
759 internalization. Neuron. 25(3):649–662. doi:10.1016/s0896-6273(00)81067-3.

760 McColl G, Rogers AN, Alavez S, Hubbard AE, Melov S, Link CD, Bush AI, Kapahi P, Lithgow
761 GJ. 2010. Insulin-like Signaling Determines Survival During Stress via Post Transcriptional
762 Mechanisms in C. elegans. Cell Metab. 12(3):260–272. doi:10.1016/j.cmet.2010.08.004.

763 McElwee J, Bubb K, Thomas JH. 2003. Transcriptional outputs of the Caenorhabditis elegans
764 forkhead protein DAF-16. Aging Cell. 2(2):111–121. doi:10.1046/j.1474-9728.2003.00043.x.

765 Mello C, Fire A. 1995. DNA transformation. Methods Cell Biol. 48:451–482.

766 Mielke JG, Taghibiglou C, Liu L, Zhang Y, Jia Z, Adeli K, Wang YT. 2005. A biochemical and
767 functional characterization of diet-induced brain insulin resistance. J Neurochem. 93(6):1568–
768 1578. doi:10.1111/j.1471-4159.2005.03155.x.

769 Momma K, Homma T, Isaka R, Sudevan S, Higashitani A. 2017. Heat-Induced Calcium
770 Leakage Causes Mitochondrial Damage in *Caenorhabditis elegans* Body-Wall Muscles.
771 Genetics. 206(4):1985–1994. doi:10.1534/genetics.117.202747.

772 Morris JZ, Tissenbaum HA, Ruvkun G. 1996. A phosphatidylinositol-3-OH kinase family
773 member regulating longevity and diapause in Caenorhabditis elegans. Nature. 382(6591):536–
774 539. doi:10.1038/382536a0.

775 Murphy CT. 2013 Dec 26. Insulin/insulin-like growth factor signaling in C. elegans.
776 WormBook.:1–43. doi:10.1895/wormbook.1.164.1.

777 Murphy CT, McCarroll SA, Bargmann CI, Fraser A, Kamath RS, Ahringer J, Li H, Kenyon C.
778 2003. Genes that act downstream of DAF-16 to influence the lifespan of Caenorhabditis elegans.
779 Nature. 424(6946):277–283. doi:10.1038/nature01789.

780 Nelson TJ, Cavallaro S, Yi CL, McPhie D, Schreurs BG, Gusev PA, Favit A, Zohar O, Kim J,
781 Beushausen S, et al. 1996. Calexcitin: a signaling protein that binds calcium and GTP, inhibits
782 potassium channels, and enhances membrane excitability. Proc Natl Acad Sci U S A.
783 93(24):13808–13813. doi:10.1073/pnas.93.24.13808.

784 Nelson TJ, Zhao W-Q, Yuan S, Favit A, Pozzo-Miller L, Alkon DL. 1999. Calexcitin interaction
785 with neuronal ryanodine receptors. :11.

786 Nieto-Estévez V, Defterali Ç, Vicario-Abejón C. 2016. IGF-I: A Key Growth Factor that
787 Regulates Neurogenesis and Synaptogenesis from Embryonic to Adult Stages of the Brain. Front
788 Neurosci. 10:52. doi:10.3389/fnins.2016.00052.

789 Oda S, Tomioka M, Iino Y. 2011. Neuronal plasticity regulated by the insulin-like signaling
790 pathway underlies salt chemotaxis learning in *Caenorhabditis elegans*. J Neurophysiol.
791 106(1):301–308. doi:10.1152/jn.01029.2010.

792 Ogg S, Paradis S, Gottlieb S, Patterson GI, Lee L, Tissenbaum HA, Ruvkun G. 1997. The Fork
793 head transcription factor DAF-16 transduces insulin-like metabolic and longevity signals in C.
794 elegans. Nature. 389(6654):994–999. doi:10.1038/40194.

795 Oh KH, Kim H. 2013. Reduced IGF signaling prevents muscle cell death in a *Caenorhabditis*
796 *elegans* model of muscular dystrophy. Proc Natl Acad Sci. 110(47):19024–19029.
797 doi:10.1073/pnas.1308866110.

798 Pan C-L, Peng C-Y, Chen C-H, McIntire S. 2011. Genetic analysis of age-dependent defects of
799 the Caenorhabditis elegans touch receptor neurons. Proc Natl Acad Sci U S A. 108(22):9274–
800 9279. doi:10.1073/pnas.1011711108.

801 Paradis S, Ailion M, Toker A, Thomas JH, Ruvkun G. 1999. A PDK1 homolog is necessary and
802 sufficient to transduce AGE-1 PI3 kinase signals that regulate diapause in Caenorhabditis
803 elegans. Genes Dev. 13(11):1438–1452. doi:10.1101/gad.13.11.1438.

804 Paradis S, Ruvkun G. 1998. Caenorhabditis elegans Akt/PKB transduces insulin receptor-like
805 signals from AGE-1 PI3 kinase to the DAF-16 transcription factor. Genes Dev. 12(16):2488–
806 2498. doi:10.1101/gad.12.16.2488.

807 Pierce SB, Costa M, Wisotzkey R, Devadhar S, Homburger SA, Buchman AR, Ferguson KC,
808 Heller J, Platt DM, Pasquinelli AA, et al. 2001. Regulation of DAF-2 receptor signaling by
809 human insulin and ins-1, a member of the unusually large and diverse C. elegans insulin gene
810 family. Genes Dev. 15(6):672–686. doi:10.1101/gad.867301.

811 Piñero González J, Carrillo Farnés O, Vasconcelos ATR, González Pérez A. 2009. Conservation
812 of key members in the course of the evolution of the insulin signaling pathway. Biosystems.
813 95(1):7–16. doi:10.1016/j.biosystems.2008.06.003.

814 Plum L, Ma X, Hampel B, Balthasar N, Coppari R, Münzberg H, Shanabrough M, Burdakov D,
815 Rother E, Janoschek R, et al. 2006. Enhanced PIP3 signaling in POMC neurons causes KATP
816 channel activation and leads to diet-sensitive obesity. J Clin Invest. 116(7):1886–1901.
817 doi:10.1172/JCI27123.

818 Rask-Madsen C, Kahn CR. 2012. Tissue–Specific Insulin Signaling, Metabolic Syndrome, and
819 Cardiovascular Disease. Arterioscler Thromb Vasc Biol. 32(9):2052–2059.
820 doi:10.1161/ATVBAHA.111.241919.

821 Rasulova M, Zečić A, Monje Moreno JM, Vandemeulebroucke L, Dhondt I, Braeckman BP.
822 2021. Elevated Trehalose Levels in C. elegans daf-2 Mutants Increase Stress Resistance, Not
823 Lifespan. Metabolites. 11(2):105. doi:10.3390/metabo11020105.

824 Roy C, Molin L, Alcolei A, Solyga M, Bonneau B, Vachon C, Bessereau J, Solari F. 2022. DAF-
825 2/insulin IGF-1 receptor regulates motility during aging by integrating opposite signaling from
826 muscle and neuronal tissues. Aging Cell. 21(8). doi:10.1111/acel.13660. [accessed 2022 Sep 19].
827 https://onlinelibrary.wiley.com/doi/10.1111/acel.13660.

828 Schindelin J, Arganda-Carreras I, Frise E, Kaynig V, Longair M, Pietzsch T, Preibisch S,
829 Rueden C, Saalfeld S, Schmid B, et al. 2012. Fiji: an open-source platform for biological-image
830 analysis. Nat Methods. 9(7):676–682. doi:10.1038/nmeth.2019.

831 Schuster E, McElwee JJ, Tullet JMA, Doonan R, Matthijssens F, Reece-Hoyes JS, Hope IA,
832 Vanfleteren JR, Thornton JM, Gems D. 2010. DamID in *C. elegans* reveals longevity-associated
833 targets of DAF-16/FoxO. Mol Syst Biol. 6(1):399. doi:10.1038/msb.2010.54.

834 Sordillo A, Bargmann CI. 2021. Behavioral control by depolarized and hyperpolarized states of
835 an integrating neuron. eLife. 10:e67723. doi:10.7554/eLife.67723.

836 Spencer WC, McWhirter R, Miller T, Strasbourger P, Thompson O, Hillier LW, Waterston RH,
837 Iii DMM. 2014. Isolation of Specific Neurons from C. elegans Larvae for Gene Expression
838 Profiling. PLOS ONE. 9(11):e112102. doi:10.1371/journal.pone.0112102.

839 Sternberg PW, Van Auken K, Wang Q, Wright A, Yook K, Zarowiecki M, Arnaboldi V, Becerra
840 A, Brown S, Cain S, et al. 2024. WormBase 2024: status and transitioning to Alliance
841 infrastructure. Genetics. 227(1):iyae050. doi:10.1093/genetics/iyae050.

842 Suh J, Hutter H. 2012. A survey of putative secreted and transmembrane proteins encoded in the
843 C. elegans genome. BMC Genomics. 13:333. doi:10.1186/1471-2164-13-333.

844 Tank EMH, Rodgers KE, Kenyon C. 2011. Spontaneous age-related neurite branching in
845 Caenorhabditis elegans. J Neurosci Off J Soc Neurosci. 31(25):9279–9288.
846 doi:10.1523/JNEUROSCI.6606-10.2011.

847 Tepper RG, Ashraf J, Kaletsky R, Kleemann G, Murphy CT, Bussemaker HJ. 2013. PQM-1
848 Complements DAF-16 as a Key Transcriptional Regulator of DAF-2-Mediated Development and
849 Longevity. Cell. 154(3):676–690. doi:10.1016/j.cell.2013.07.006.

850 Tomioka M, Adachi T, Suzuki H, Kunitomo H, Schafer WR, Iino Y. 2006. The Insulin/PI 3-
851 Kinase Pathway Regulates Salt Chemotaxis Learning in Caenorhabditis elegans. Neuron.
852 51(5):613–625. doi:10.1016/j.neuron.2006.07.024.

853 Tomioka M, Naito Y, Kuroyanagi H, Iino Y. 2016. Splicing factors control C. elegans
854 behavioural learning in a single neuron by producing DAF-2c receptor. Nat Commun. 7:11645.
855 doi:10.1038/ncomms11645.

856 Toth ML, Melentijevic I, Shah L, Bhatia A, Lu K, Talwar A, Naji H, Ibanez-Ventoso C, Ghose
857 P, Jevince A, et al. 2012. Neurite sprouting and synapse deterioration in the aging Caenorhabditis
858 elegans nervous system. J Neurosci Off J Soc Neurosci. 32(26):8778–8790.
859 doi:10.1523/JNEUROSCI.1494-11.2012.

860 Weng Y, Zhou S, Morillo K, Kaletsky R, Lin S, Murphy CT. 2024. The neuron-specific
861 IIS/FOXO transcriptome in aged animals reveals regulatory mechanisms of cognitive aging.
862 eLife. 13:RP95621. doi:10.7554/eLife.95621.

863 Zhang P, Judy M, Lee S-J, Kenyon C. 2013. Direct and Indirect Gene Regulation by a Life-
864 Extending FOXO Protein in C. elegans: Roles for GATA Factors and Lipid Gene Regulators.
865 Cell Metab. 17(1):85–100. doi:10.1016/j.cmet.2012.12.013.

866 Zhao Y, Zhang B, Marcu I, Athar F, Wang H, Galimov ER, Chapman H, Gems D. 2021.
867 Mutation of daf-2 extends lifespan via tissue-specific effectors that suppress distinct life-limiting
868 pathologies. Aging Cell. 20(3):e13324. doi:10.1111/acel.13324.

869 Zhu R, Chin-Sang ID. 2024. C. elegans insulin-like peptides. Mol Cell Endocrinol. 585:112173.
870 doi:10.1016/j.mce.2024.112173.

871

872 **Figure 1. DAF-16 activity in different genetic backgrounds for mRNA-seq.**
873 (a) The effect of insulin/IGF-1 signaling (IIS) state on DAF-16 activity. A schematic of the IIS
874 pathway in *C. elegans* is shown. Phosphorylation of DAF-16 sequesters the FOXO transcription
875 factor from the nucleus, inhibiting DAF-16-directed transcriptional regulation. (b) Schematic of
876 the FACS/mRNA-seq workflow for data collection. Animals of different genotypes (wild-type,
877 *daf-16(lf)*, *daf-2(lf)*, *daf-16(lf); daf-2(lf)*) express GFP specifically in the body wall muscle cells.
878 Age-matched young adults were collected, and cells were dissociated before being subjected to
879 FACS. GFP+; PI- (propidium iodide negative) cells were sorted as 'muscle cells', whereas PI-
880 cells were collected as 'all cells'. Total mRNA was isolated for sequencing. (c) Principal
881 component analysis (PCA) of the mRNA-seq datasets from 24 samples. (d) PCA of the mRNA-
882 seq datasets from 12 *daf-2(lf)* samples (top) and 12 *daf-2(+)* samples (bottom).
883
884 **Figure 2. Differential gene expression analyses across transcriptomes of eight genotypes.**
885 (a, b) Volcano plots of differentially expressed genes (DEGs) for muscle cells at high IIS state,
886 by comparing 'muscle cell' samples from wild-type and *daf-16(lf)* animals (a), for muscle cells
887 at low IIS state, by comparing 'muscle cell' samples from *daf-2(lf)* and *daf-16(lf); daf-2(lf)*
888 animals (b). Grey dots denote genes deemed unaffected by DAF-16 (FDR > 0.05). Red and blue
889 dots denote genes upregulated and downregulated, respectively, by DAF-16 (FDR < 0.05). Red
890 and blue dots with transparency denote those with <4 counts per million (CPM). Triangles
891 denote values that exceed the scale at either axes. (c) Heatmap representation of transcript
892 abundance of the 139 candidates for muscle-specific DAF-16-dependent transcriptional changes
893 by mRNA-seq analyses. Transcript abundance in 'muscle cells' (left) and 'all cells' (right) were
894 compared between four genetic backgrounds: wild-type, *daf-16(lf)*, *daf-2(lf)*, and *daf-16(lf); daf-*
895 *2(lf)*. Transcript abundance was hierarchically clustered by similarities. Colors correspond to the
896 z-score normalized over the average transcript abundance of each gene across all samples.
897
898 **Figure 3. Combined DAF-16 ChIP-seq and comparative mRNA-seq analyses**.
899 (a) GFP::DAF-16a binding sites per chromosome, by two datasets for intestine ChIP-seq (grey)
900 and one dataset for muscle ChIP-seq (brown). Peak numbers were binned for every 100,000 base
901 pairs. (b) A volcano plot of 312 differentially expressed genes (DEGs) in muscle cells, by
902 comparing 'muscle cells' samples from *daf-2(lf)* and *daf-16(lf); daf-2(lf)* animals. Grey dots

903 denote genes without a muscle DAF-16 binding site within 5 kb flanking both sides of its coding
904 region. Red and blue dots denote genes upregulated and downregulated, respectively, with a
905 muscle DAF-16 binding site. Colored dots with denoted gene names have DAF-16 binding sites
906 that are absent from both intestine ChIP-seq datasets. (c) A summary of our workflow to
907 prioritize muscle-specific DAF-16 targets.
908
909 **Figure 4. Muscle-specific upregulation of *C54F6.5* by DAF-16.**
910 (a) *C54F6.5* expression levels, measured as mRNA-seq read counts per million (CPM), across
911 genetic backgrounds and cell types. (b) Fold changes of *C54F6.5* expression in respective
912 genetic backgrounds, normalized against the wild-type level by RT-qPCR. Each data point
913 represents the average of three cDNA dilutions (500pg, 5ng, and 50ng) from a single trial. n = 3
914 for all four genotypes. (c) The genomic structure of *C54F6.5* with its ChIP-seq peak, DAF-16
915 binding element (DBE), and reporter design labeled. (d) Representative confocal images and
916 quantification of a *C54F6.5* transcriptional reporter in different genetic backgrounds. n = 19, 19,
917 19, 16. (e) Representative confocal images and quantification of a *C54F6.5* translational reporter
918 with its endogenous 3' UTR in different genetic backgrounds. n = 16, 17, 20, 10. (f)
919 Representative confocal images and quantification of a *C54F6.5* transcriptional reporter with its
920 endogenous 3' UTR in different genetic backgrounds. n = 15, 13, 13, 12. BWM: body wall
921 muscle. SP: spermatheca. All scale bars = 50 um. Non-significant comparisons were not labeled.
922 **** $p < 0.0001$. ** $p < 0.01$. * $p < 0.05$. Error bars: standard deviation.
923
924 **Figure 5. Muscle-specific upregulation of *cex-1* by DAF-16.**
925 (a) *cex-1* transcript abundance, measured as mRNA-seq read counts per million (CPM), across
926 genetic backgrounds and cell types. Each dot represents the CPM from one sample. (b) Fold
927 changes of *cex-1* expression in respective genetic backgrounds, normalized against the wild-type
928 level by RT-qPCR. Each data point represents the average of three cDNA dilutions (500pg, 5ng,
929 and 50ng) from a single trial. n = 3 for all four genotypes. (c) The genomic structure of *cex-1*
930 with its ChIP-seq peak, DAF-16 binding element (DBE), and reporter design labeled. (d)
931 Representative confocal images and quantification of a *cex-1* transcriptional reporter with its
932 endogenous 3' UTR in respective genetic backgrounds. n = 16, 14, 17, 14 animals for muscle. n
933 = 16, 11, 11, 13 animals for RIM. (e) Representative confocal images and quantification of a *cex-*

934 *1* endogenous reporter in respective genetic backgrounds. Each dot represents the image intensity
935 for area of interest for one animal. n = 24, 22, 26, 25 animals for muscle. n = 23, 23, 29, 28
936 animals for RIM. BWM: body wall muscle; PM: pharyngeal muscle. All scale bars = 50 um.
937 Non-significant comparisons were not labeled. **** $p < 0.0001$. Error bars: standard deviation.
938
939 **Figure 6. Muscle-specific upregulation of *mlcd-1* by DAF-16.**
940 (a) *mlcd-1* expression levels, measured as mRNA-seq read counts per million (CPM), across
941 genetic backgrounds and cell types. (b) The genomic structure of *mlcd-1* with its ChIP-seq peak,
942 DAF-16 binding element (DBE), and reporter design labeled. (c) Representative confocal images
943 and quantification of an *mlcd-1* transcriptional reporter with its endogenous 3' UTR in respective
944 genetic backgrounds. n = 15, 15, 17, 16. BWM: body wall muscle. Scale bar = 50 um. Non-
945 significant comparisons were not labeled. ** $p < 0.01$. Error bars: standard deviation.

946 **Table 1. DAF-16-dependent transcriptional regulation candidates at high IIS state**

	Salmon muscle CPM (mean±SD, n=4)		**STAR-HTSeq muscle CPM (mean±SD, n=4)**		**DESeq2 based on Salmon**	
Gene	**wild-type**	***daf-16(lf)***	**wild-type**	***daf-16(lf)***	**log2 fold change**	**adjusted p-value**
col-33	0.16±0.15	30.53±46.51	0.17±0.16	34.47±52.29	-7.10	6.32E-08
ZK105.1	15.86±7.03	4.06±2.11	18.27±6.84	4.59±1.98	2.00	2.58E-03
*daf-16**	23.08±6.49	11.30±8.73	24.17±6.70	11.74±8.99	0.99	2.92E-02
Genes excluded due to low reads						
gcy-3	0.02±0.03	0±0	0.02±0.02	0±0	17.27	2.11E-16
F23B2.10	0.01±0.02	0±0	0.03±0.04	0±0	15.99	3.82E-12
flr-4	0.86±1.15	0.05±0.03	0.89±1.24	0.08±0.07	3.87	2.34E-02
C55C3.3	3.57±2.17	0.49±0.40	3.93±2.51	0.51±0.39	2.93	5.47E-03
fpn-1.2	0.54±0.43	0.08±0.03	0.66±0.38	0.08±0.04	2.67	2.48E-02
C10F3.7	0.03±0.04	3.63±6.49	0.02±0.04	3.62±6.42	-5.90	1.05E-02
srbc-15	0.01±0.02	2.17±2.99	0.01±0.02	1.86±2.41	-6.75	2.86E-02
Y6B3B.1	0±0	0.07±0.12	0±0	0.06±0.11	-17.86	1.67E-23
fbxb-33	0±0	1.75±3.48	0±0	0.01±0.01	-28.14	2.15E-04

947 *: Excluded from the candidate list of DAF-16-regulation events. Reduced reads resulted from
948 the loss of transcription in the deleted genomic region in the *daf-16(mu86)* allele.

949 **Table 2. A summary of sequentially applied criteria for candidate DAF-16 targets**

Candidates	Description	Criteria (FDR < 0.05)
195 (Table S3)	DAF-16-dependent transcript changes present in muscle cells	'muscle cells' *daf-2(lf)* **vs** wild-type, *daf-16(lf)*, and *daf-16(lf); daf-2(lf)*
139 (Table S4)	DAF-16-dependent transcript changes enriched for muscle cells	overlap with *daf-2(lf)* 'muscle cells' **vs** wild-type, *daf-16(lf)*, *daf-2(lf)*, *daf-16(lf); daf-2(lf)* 'all cells'
55 (Table S6)	Muscle-enriched DAF-16-dependent transcript changes with DAF-16a binding	with DAF-16a binding detected in a muscle ChIP-seq dataset (Table S5)
12 (Table 3)	Candidate for muscle-specific DAF-16 target	without DAF-16a binding detected in 2 intestine ChIP-seq datasets (Table S5)

950

951 **Table 3. Twelve muscle-specific DAF-16 target candidates**

	muscle cell CPM (mean±SD, n=3; Salmon)		**muscle cell CPM (mean±SD, n=3; STAR-HTSeq)**		**DESeq2 based on Salmon**	
Gene	***daf-2****(lf)*	***daf-16****(lf);* ***daf-2****(lf)*	***daf-2****(lf)*	***daf-16****(lf);* ***daf-2****(lf)*	**log2 fold change**	**adjusted p-value**
C54F6.5	30.63±17.11	0.84±0.51	32.82±17.93	0.87±0.55	5.52	6.10E-12
cex-1	737.98±235.3	168.9±38.31	771.67±254.42	173.65±41.31	2.40	8.08E-07
gstk-2	23.32±3.34	5.03±0.82	22.01±3.94	5.39±0.82	2.33	4.56E-02
mlcd-1	29.8±3.52	11.91±5.59	26.39±3.56	10.72±5.07	1.72	9.91E-04
Genes not tested due to moderate fold changes for transcripts of high/moderate abundance						
act-2	940.04±471.42	386.24±130.45	749.3±375.8	298.78±102.85	1.59	1.90E-03
F23D12.7	105.27±24.15	46.76±11.32	110.53±25.16	47.56±11.5	1.29	4.52E-02
tiar-3	45.43±11.5	22.35±4.81	49.41±12	23.71±5.69	1.29	2.65E-03
Y43F8B.1	1475.99±257.45	677.98±58.46	1547.34±272.86	695.17±62.1	1.20	4.39E-02
unc-78	338.08±17.49	200.69±36.39	351.32±20.26	204.05±38.8	0.97	2.44E-02
ksr-1	29.31±10.06	17.7±3.00	30.5±10.45	17.93±3.11	0.97	4.02E-02
aqp-2	585.75±155.07	414.25±114.85	606.98±154.31	421.93±120.2	0.78	4.79E-02
goa-1	225.55±42.3	172.71±45.62	235.42±46.7	176.81±48.57	0.66	3.78E-02
Genes excluded due to low reads						
alh-2	1.95±2.44	0±0	2.24±2.88	0±0	8.88	8.06E-04
rap-3	0.01±0.02	0.4±0.24	0.01±0.02	0.41±0.2	-4.95	1.15E-02

952

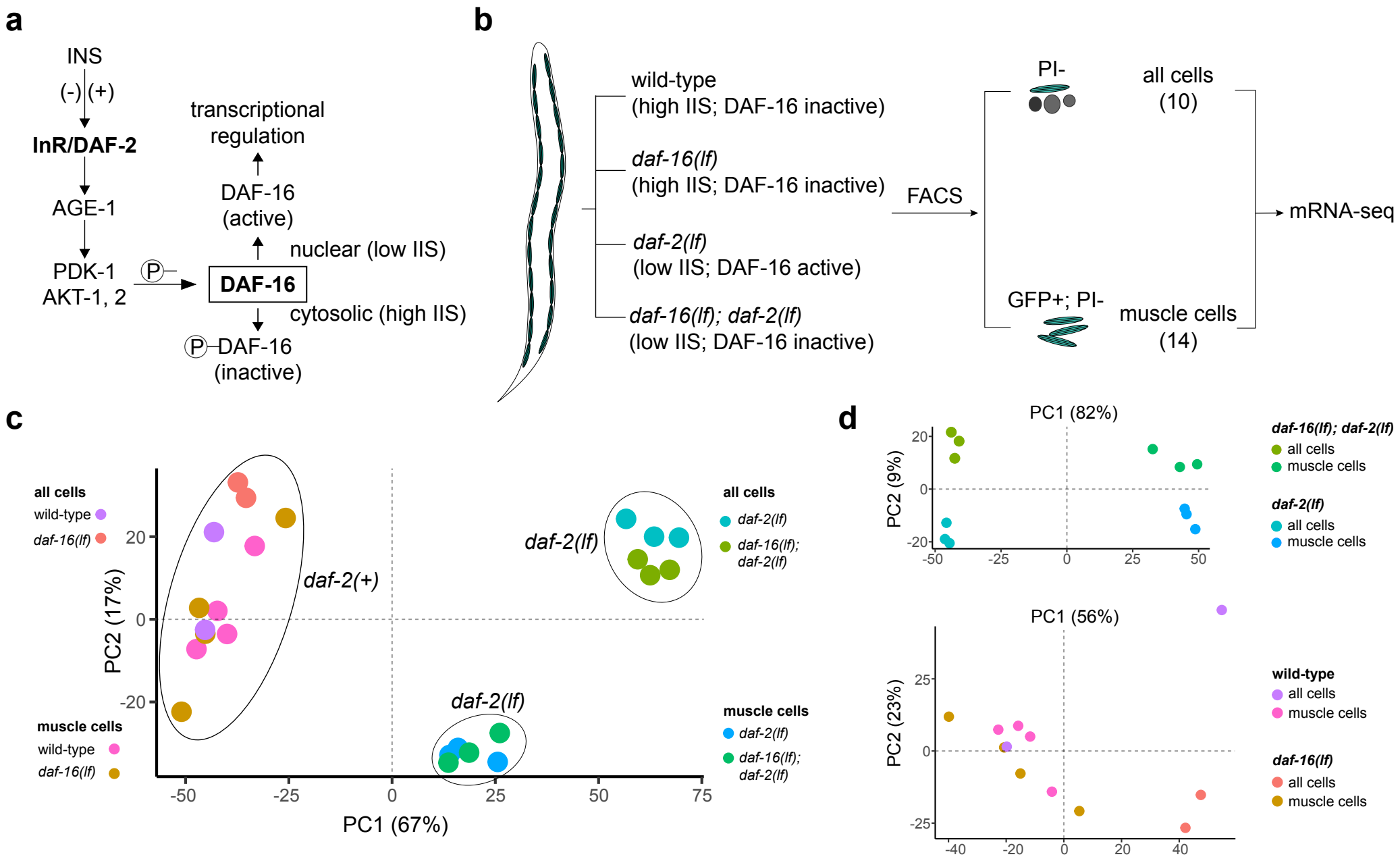
a
INS
(-) (+)
InR/DAF-2
AGE-1
PDK-1
AKT-1, 2
P
DAF-16
transcriptional regulation
DAF-16 (active)
nuclear (low IIS)
cytosolic (high IIS)
P DAF-16 (inactive)
b
wild-type (high IIS; DAF-16 inactive)
daf-16(lf) (high IIS; DAF-16 inactive)
daf-2(lf) (low IIS; DAF-16 active)
daf-16(lf); daf-2(lf) (low IIS; DAF-16 inactive)
FACS
PI-
all cells (10)
GFP+; PI-
muscle cells (14)
mRNA-seq
c
all cells
wild-type
daf-16(lf)
muscle cells
wild-type
daf-16(lf)
daf-2(+)
daf-2(lf)
daf-2(lf)
all cells
daf-2(lf)
daf-16(lf); daf-2(lf)
muscle cells
daf-2(lf)
daf-16(lf); daf-2(lf)
PC2 (17%)
PC1 (67%)
d
PC1 (82%)
PC2 (9%)
daf-16(lf); daf-2(lf)
all cells
muscle cells
daf-2(lf)
all cells
muscle cells
PC1 (56%)
PC2 (23%)
wild-type
all cells
muscle cells
daf-16(lf)
all cells
muscle cells

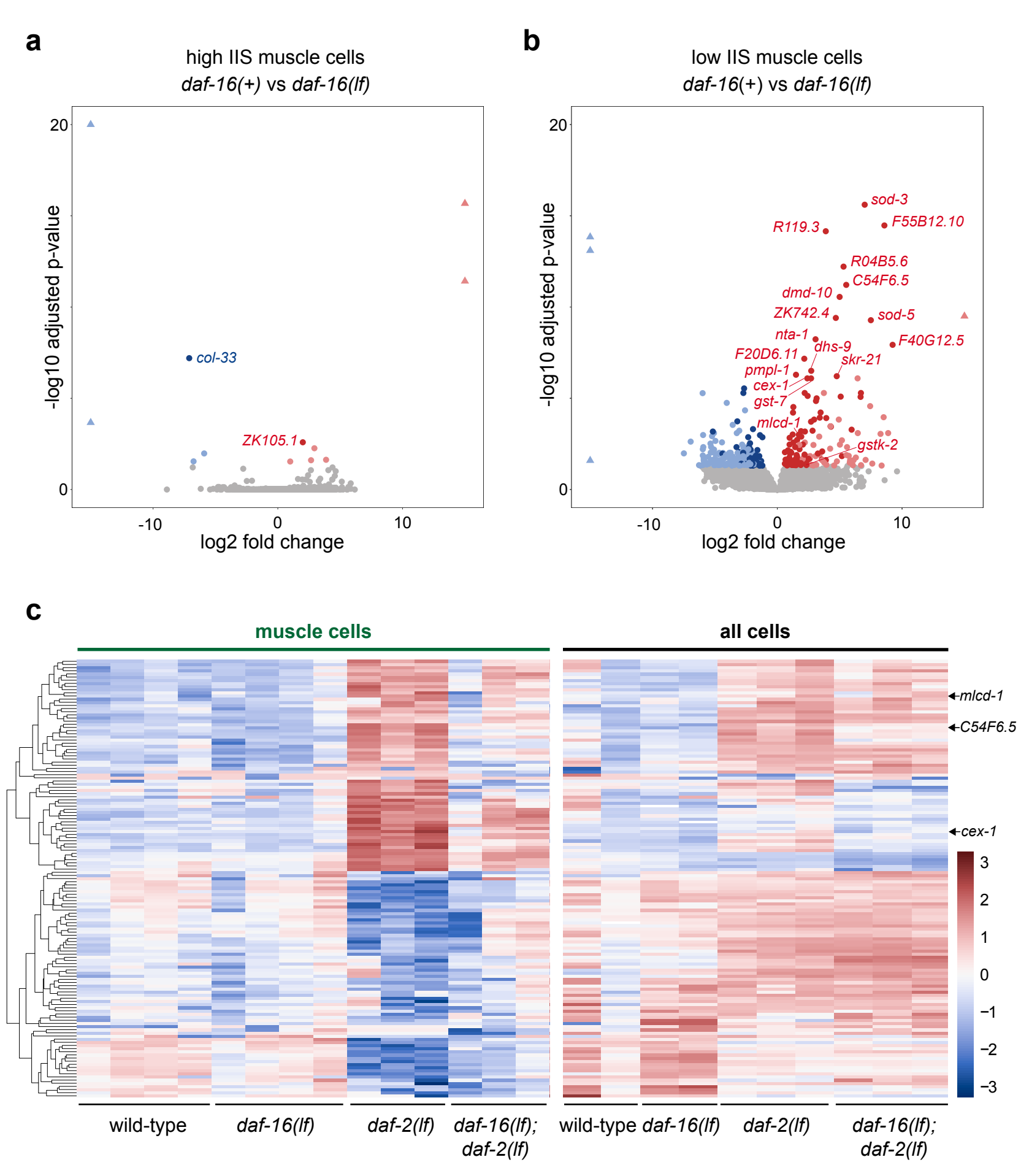
a
high IIS muscle cells
daf-16(+) vs daf-16(lf)
-log10 adjusted p-value
log2 fold change
col-33
ZK105.1
b
low IIS muscle cells
daf-16(+) vs daf-16(lf)
sod-3
F55B12.10
R119.3
R04B5.6
C54F6.5
dmd-10
ZK742.4
sod-5
nta-1
F40G12.5
dhs-9
F20D6.11
skr-21
pmpl-1
cex-1
gst-7
mlcd-1
gstk-2
c
muscle cells
all cells
mlcd-1
C54F6.5
cex-1
wild-type
daf-16(lf)
daf-2(lf)
daf-16(lf); daf-2(lf)

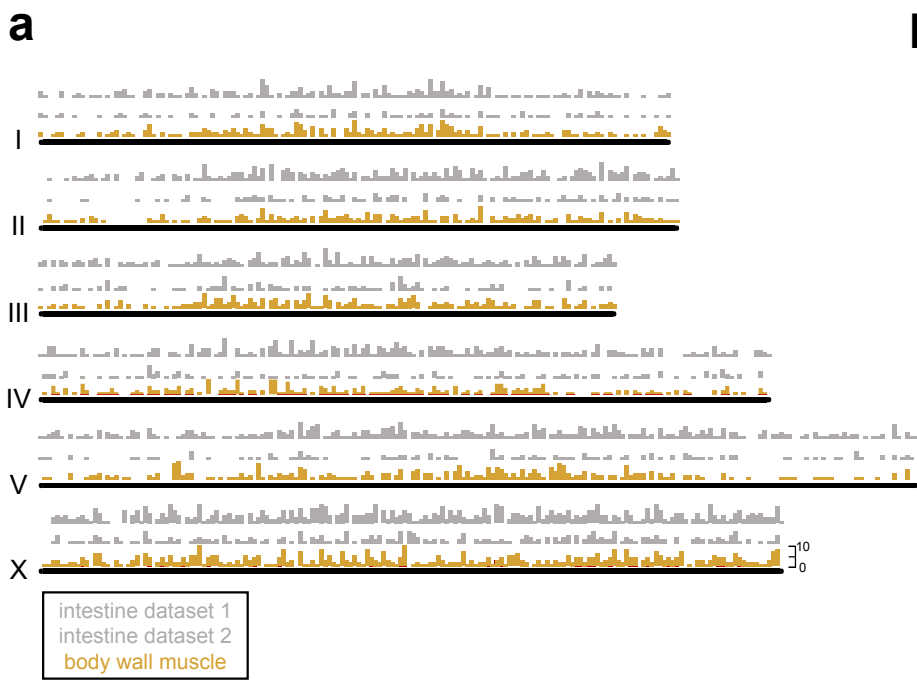
a
I
II
III
IV
V
X
10
0
intestine dataset 1
intestine dataset 2
body wall muscle

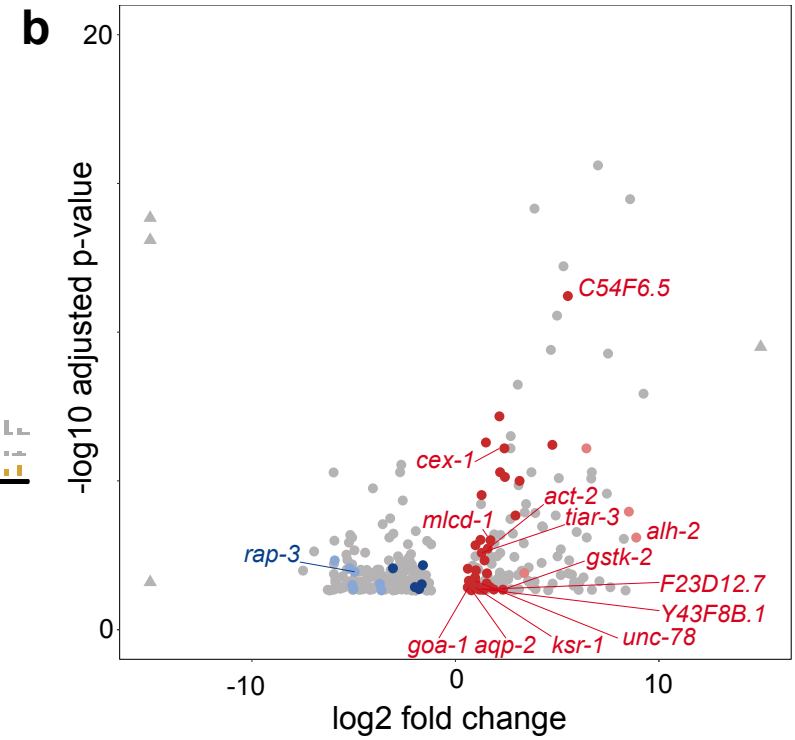
b
20
0
-log10 adjusted p-value
-10
0
10
log2 fold change
C54F6.5
cex-1
act-2
mlcd-1
tiar-3
alh-2
rap-3
gstk-2
F23D12.7
Y43F8B.1
goa-1
aqp-2
ksr-1
unc-78

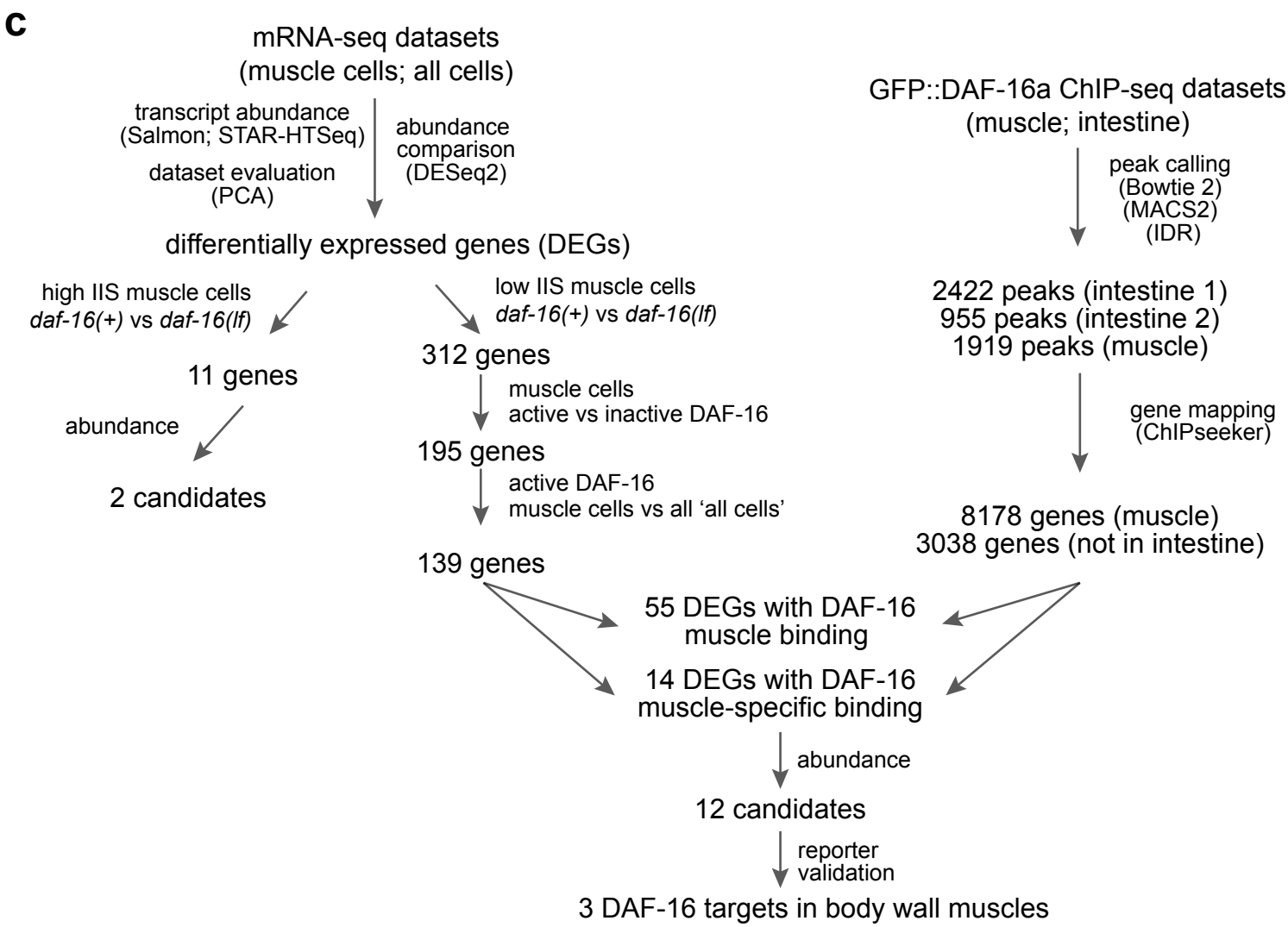
c
mRNA-seq datasets
(muscle cells; all cells)
transcript abundance
(Salmon; STAR-HTSeq)
dataset evaluation
(PCA)
abundance
comparison
(DESeq2)
differentially expressed genes (DEGs)
high IIS muscle cells
daf-16(+) vs daf-16(lf)
11 genes
abundance
2 candidates
low IIS muscle cells
daf-16(+) vs daf-16(lf)
312 genes
muscle cells
active vs inactive DAF-16
195 genes
active DAF-16
muscle cells vs all 'all cells'
139 genes
GFP::DAF-16a ChIP-seq datasets
(muscle; intestine)
peak calling
(Bowtie 2)
(MACS2)
(IDR)
2422 peaks (intestine 1)
955 peaks (intestine 2)
1919 peaks (muscle)
gene mapping
(ChIPseeker)
8178 genes (muscle)
3038 genes (not in intestine)
55 DEGs with DAF-16
muscle binding
14 DEGs with DAF-16
muscle-specific binding
abundance
12 candidates
reporter
validation
3 DAF-16 targets in body wall muscles

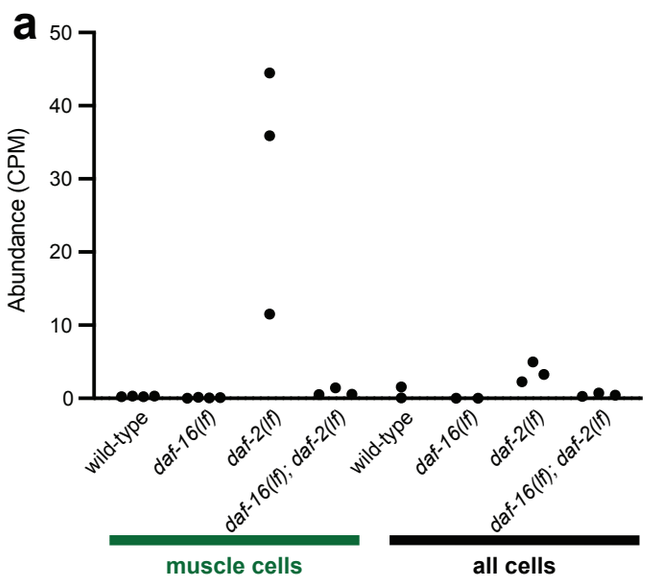
a
Abundance (CPM)
50
40
30
20
10
0
wild-type
daf-16(lf)
daf-2(lf)
daf-16(lf); daf-2(lf)
wild-type
daf-16(lf)
daf-2(lf)
daf-16(lf); daf-2(lf)
muscle cells
all cells

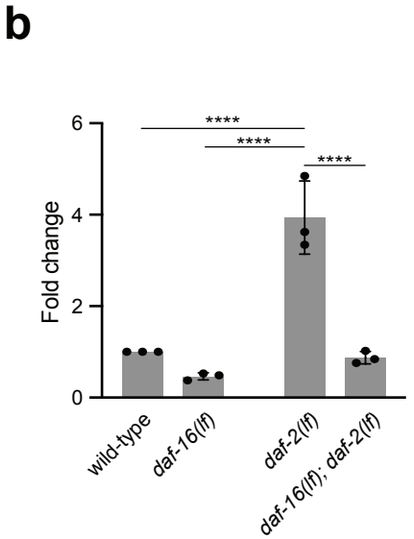
b
Fold change
6
4
2
0
****
****
****
wild-type
daf-16(lf)
daf-2(lf)
daf-16(lf); daf-2(lf)

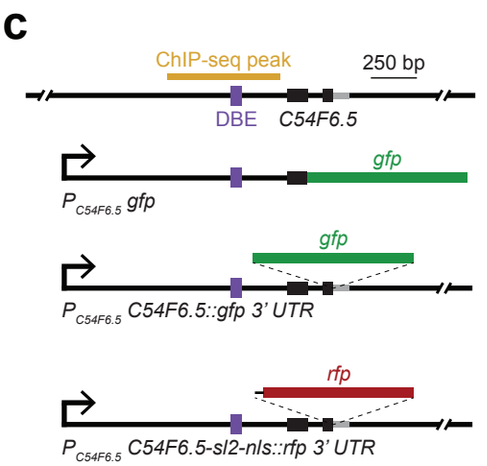
c
ChIP-seq peak
250 bp
DBE
C54F6.5
gfp
P C54F6.5 gfp
gfp
P C54F6.5 C54F6.5::gfp 3' UTR
rfp
P C54F6.5 C54F6.5-sl2-nls::rfp 3' UTR

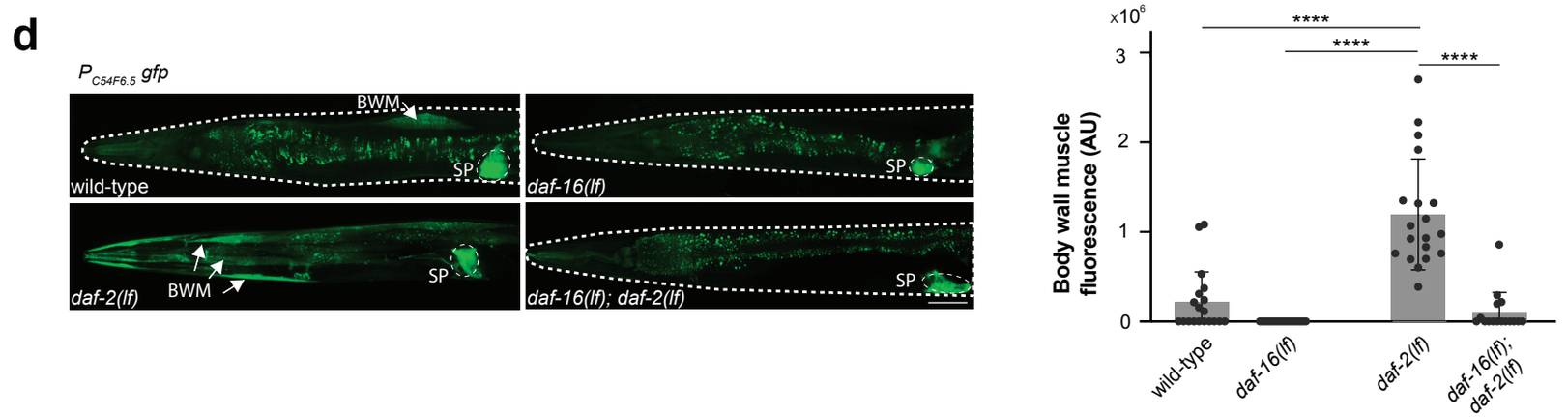
d
P C54F6.5 gfp
BWM
SP
wild-type
daf-16(lf)
daf-2(lf)
daf-16(lf); daf-2(lf)
x10^6
Body wall muscle fluorescence (AU)
3
2
1
0
****
****
****
wild-type
daf-16(lf)
daf-2(lf)
daf-16(lf); daf-2(lf)

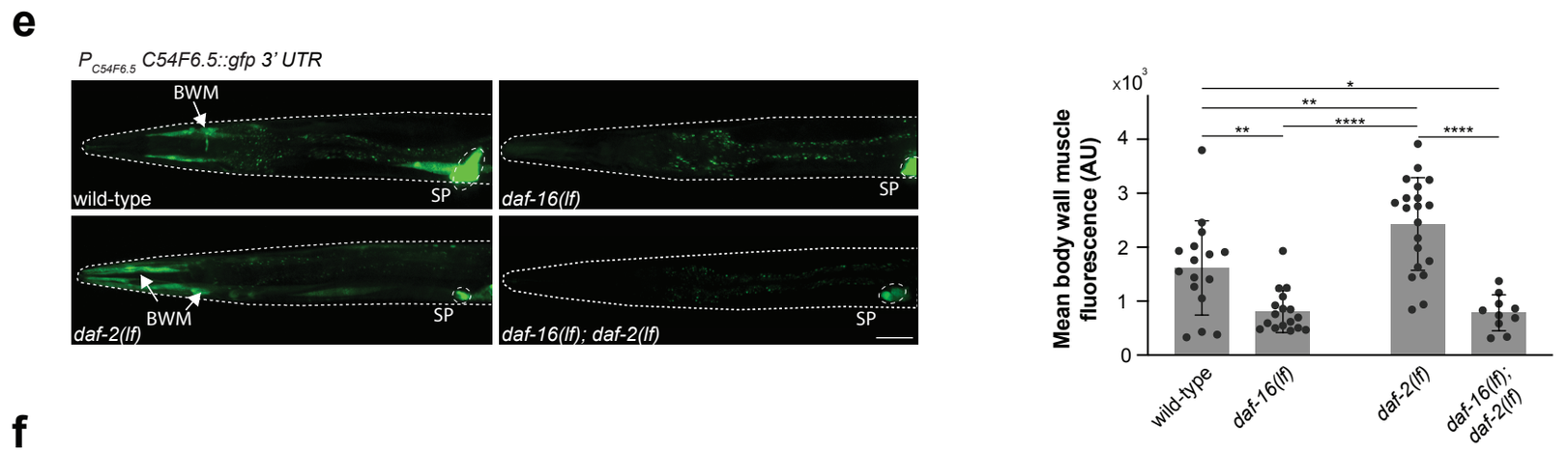
e
P C54F6.5 C54F6.5::gfp 3' UTR
BWM
SP
wild-type
daf-16(lf)
daf-2(lf)
daf-16(lf); daf-2(lf)
x10^3
Mean body wall muscle fluorescence (AU)
4
3
2
1
0
*
**
**
****
****
wild-type
daf-16(lf)
daf-2(lf)
daf-16(lf); daf-2(lf)

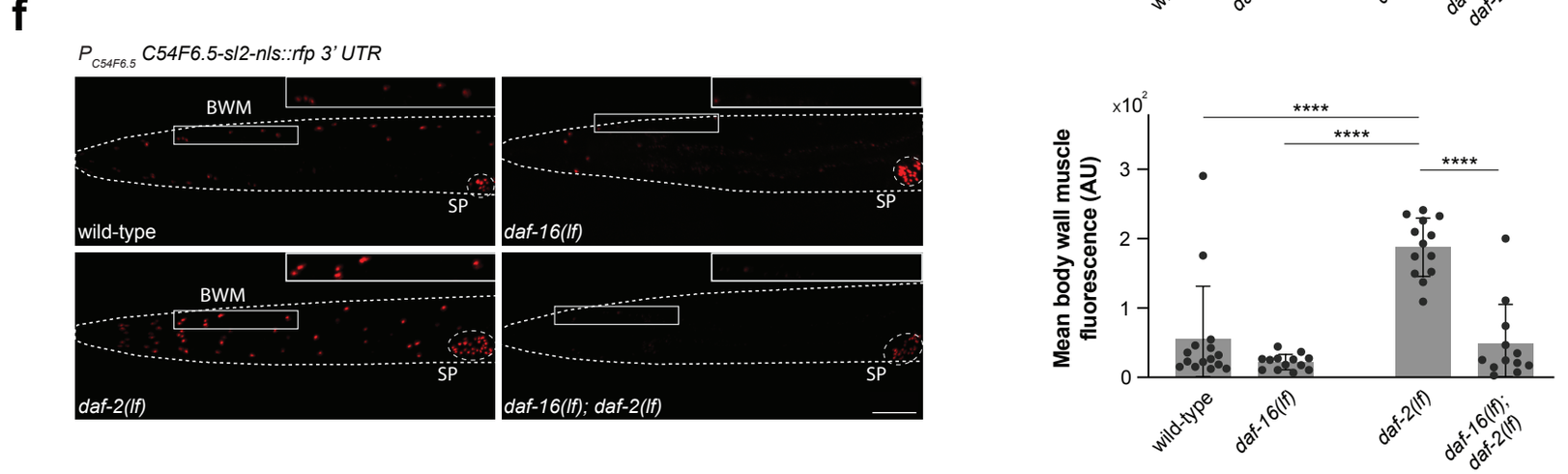
f
P C54F6.5 C54F6.5-sl2-nls::rfp 3' UTR
BWM
SP
wild-type
daf-16(lf)
daf-2(lf)
daf-16(lf); daf-2(lf)
x10^2
Mean body wall muscle fluorescence (AU)
3
2
1
0
****
****
****
wild-type
daf-16(lf)
daf-2(lf)
daf-16(lf); daf-2(lf)

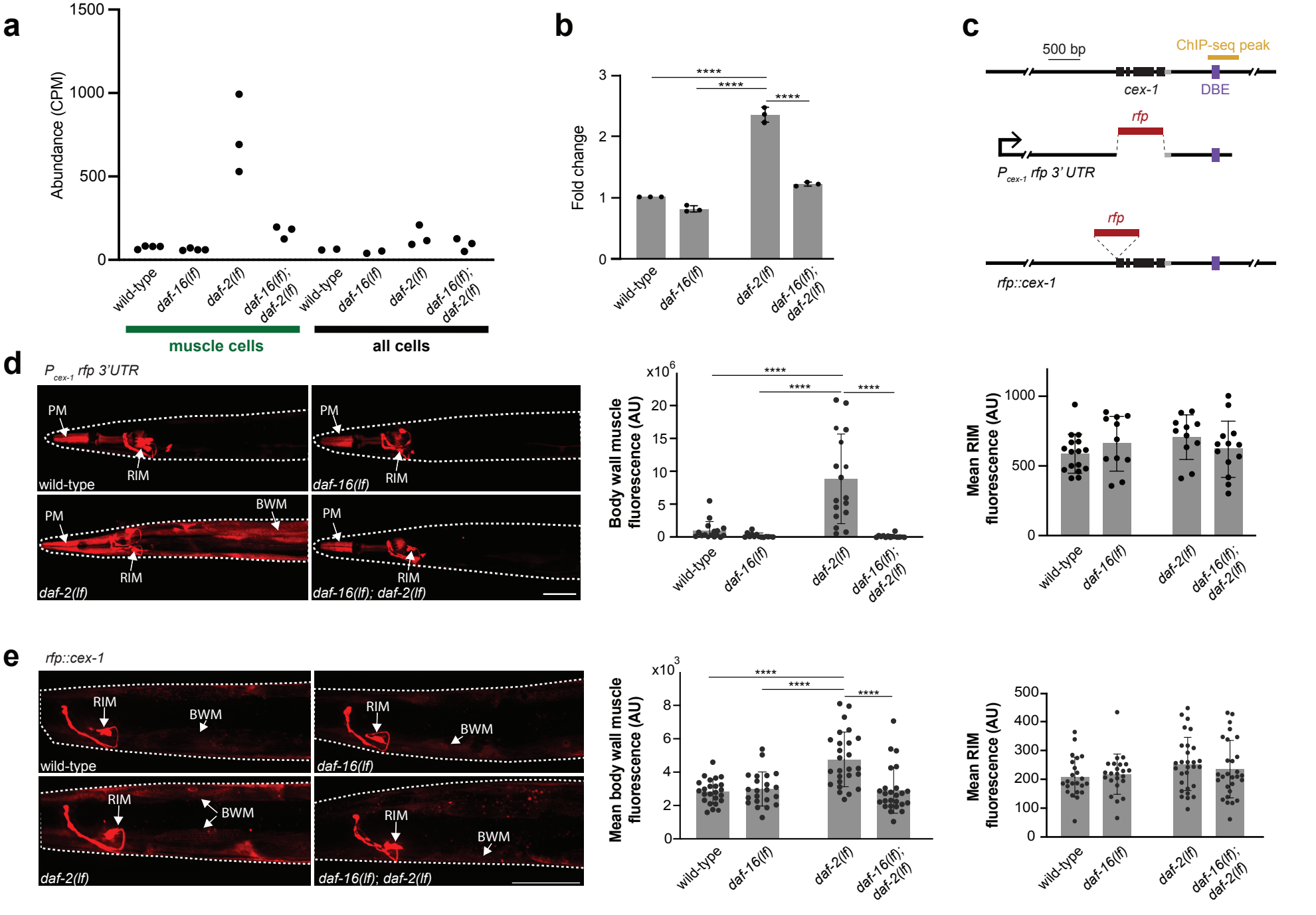
a
Abundance (CPM)
1500
1000
500
0
wild-type
daf-16(lf)
daf-2(lf)
daf-16(lf); daf-2(lf)
muscle cells
all cells
b
Fold change
****
c
500 bp
ChIP-seq peak
cex-1
DBE
rfp
P cex-1 rfp 3' UTR
rfp::cex-1
d
P cex-1 rfp 3'UTR
PM
RIM
BWM
wild-type
daf-16(lf)
daf-2(lf)
daf-16(lf); daf-2(lf)
Body wall muscle fluorescence (AU)
x10^6
Mean RIM fluorescence (AU)
e
rfp::cex-1
Mean body wall muscle fluorescence (AU)
x10^3

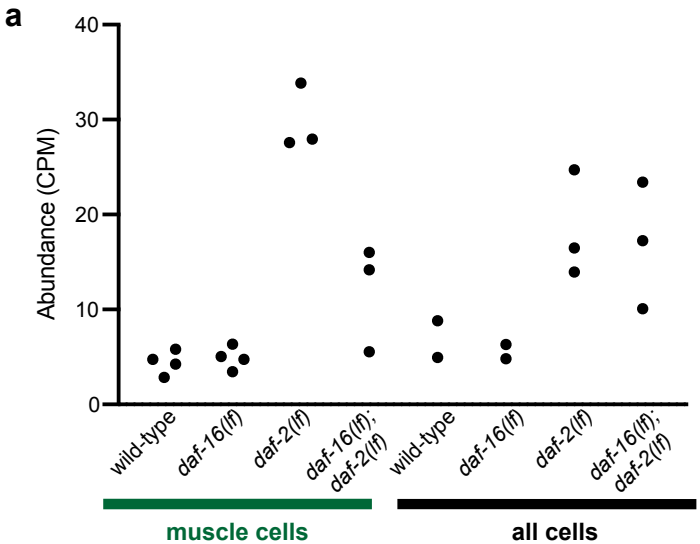
a
Abundance (CPM)
40
30
20
10
0
wild-type
daf-16(lf)
daf-2(lf)
daf-16(lf); daf-2(lf)
wild-type
daf-16(lf)
daf-2(lf)
daf-16(lf); daf-2(lf)
muscle cells
all cells

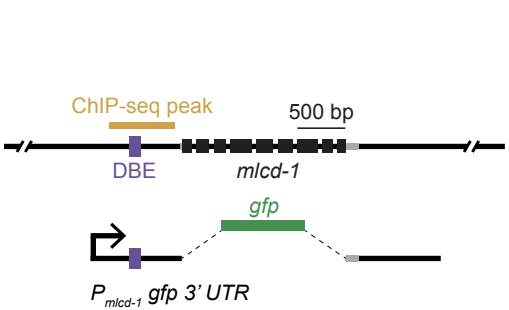
b
ChIP-seq peak
500 bp
DBE
mlcd-1
gfp
P mlcd-1 gfp 3' UTR

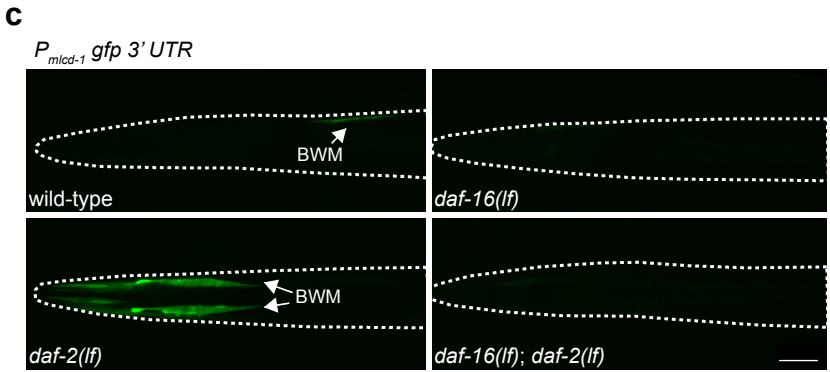
c
P mlcd-1 gfp 3' UTR
BWM
wild-type
daf-16(lf)
BWM
daf-2(lf)
daf-16(lf); daf-2(lf)

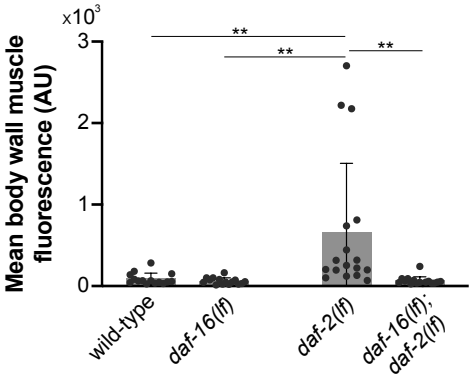
x10^3
3
2
1
0
Mean body wall muscle fluorescence (AU)
**
**
**
wild-type
daf-16(lf)
daf-2(lf)
daf-16(lf); daf-2(lf)